Hindawi
Geofluids
Volume 2020, Article ID 8883297, 23 pages
https://doi.org/10.1155/2020/8883297

Research Article

Origin of Bedding-Parallel Calcite Veins from Lacustrine Shale in the Eocene Dongying Depression, Bohai Bay Basin, China

Zhenhuan Shen,[1] Bingsong Yu,[1] Chenyang Bai,[2] Shujun Han,[1] and Huimin Liu[3]

[1]*School of Geosciences and Resources, China University of Geosciences, Beijing 100083, China*
[2]*School of Ocean Sciences, China University of Geosciences, Beijing 100083, China*
[3]*Shengli Oilfield Company, SINOPEC, Dongying, Shandong 257000, China*

Correspondence should be addressed to Bingsong Yu; yubs@cugb.edu.cn and Chenyang Bai; baicy@cugb.edu.cn

Received 11 August 2020; Revised 23 November 2020; Accepted 25 November 2020; Published 21 December 2020

Academic Editor: Timothy S. Collett

Calcite veins, which developed parallel to the bedding, are widespread in laminated source rocks in the Eocene Dongying Depression. However, there is a lack of systematic description and classification of the veins. This study presents a systematic characterization of the calcite veins, host rocks, and micritic carbonate laminae by applying petrographic and geochemical methods to understand vein-forming mechanisms. Antitaxial and syntaxial veins are examined. Antitaxial veins contain typical fibrous crystals with the most intense fluorescence, and the median zone of these veins is often the micritic carbonate. Calcite crystals in syntaxial veins develop a blocky morphology of various sizes, indicating obvious growth competition. Data of rare earth elements and trace elements obtained from the micritic laminae, host rocks, and calcite veins are very similar. This indicates that the vein-forming nutrients originated from the carbonate in the host rocks and micritic laminae. The minor difference in C and Sr isotopes between calcite veins and micritic carbonate within the host rock and the negative shift in O isotopes in the veins are caused by ion exchange and dehydration of swelling clay minerals in the burial environment. This further proves that the calcite veins are formed in a closed system. Geochemical analysis suggests that the rocks are in the oil window and have good hydrocarbon potential. Thermal evolution of the acidic fluids generated from organic matter (OM) resulted in the dissolution of carbonate and formed fluid overpressure in the rocks. Fluid overpressure induced the formation of fractures in the interlayer and expanded the veins with the force of crystallization due to fibrous calcite growth. Blocky crystals grow in the fractures from the margins toward the center. Hydrocarbon expulsed via OM maturation in the host rock fills the intercrystalline pores. Moreover, shale with bedding-parallel calcite has the characteristics of high-quality shale oil reservoirs. These characteristics will probably provide guidance for shale oil exploration.

1. Introduction

Calcite veins are common in low-permeability source rocks. In particular, bedding-parallel veins filled by fibrous calcite, in which the fibers are mutually parallel and form quasivertically, have been reported from more than 110 localities in the world [1–3]. The shape, orientation, and internal structure of calcite veins preserve abundant information on the diagenesis, palaeostress, and rock deformation [4, 5]. According to various vein types and associated crystal growth direction, morphologies, and vein growth mechanisms, Durney and Ramsay [6] distinguished stretched, syntaxial, and antitaxial veins. They can be further subdivided into blocky, elongate-blocky, and fibrous veins based on their crystal forms and arrangements [7].

Syntaxial veins often contain blocky or elongate-blocky crystals, which are ascribed to crystal growth into open holes or rapidly opening veins and exhibit strong growth competition. Since the shape of crystals cannot define the opening trail, only the total comparative displacement of the vein walls can be determined [7]. Antitaxial veins normally consist of fibrous crystals with smooth crystal boundaries [5]. Curved fiber boundaries can be used to infer the opening trail during the growth of cracks [8]. In addition, both solid inclusions detached from the vein walls and different phases of vein growth can indicate the opening process or direction

[9, 10]. Ramsay [9] proposed that the crack-seal mechanism can explain the growth of veins with elongated to fibrous crystals. Numerical simulations of fiber growth based on the crack-seal mechanism revealed that crystal growth competition is suppressed when the fracture width is less than 10 μm [11]. Therefore, the genesis of veins has been attributed to fluid overpressure caused by ascending fluid migration, which results in tensile stress in low-permeability host rocks [12, 13]. The force of crystallization and ongoing deformation can explain fibrous veins with continuous growth characteristics [14–17]. However, not all fibrous veins form by the crack-seal mechanism. Some may form without the loss of cohesion between vein fibers and host rock [15], such as solid inclusions formed by fluctuations of adhesion at the interface of the vein and host rock [17].

Secondary minerals in veins precipitate mainly from supersaturated aqueous solutions because of changes in physiochemical conditions [18]. Diffusion and advection are the fundamental material-transport mode that controls vein formation [19]. In an open system, advective flow carries the solutions over long distances until they precipitate minerals in veins [20]. In contrast, in a closed system, the solutions diffuse over shorter distances [21]. Nevertheless, diffusion always plays a vital role in the formation of relatively thicker veins [22]. The mode of transport can be inferred from the geometry of the microstructures in veins. Therefore, the mineralogical and geochemical analysis of veins can provide valuable clues regarding the origin and nature of fluids.

The Dongying Depression in eastern China is rich in oil-bearing shales in which several bedding-parallel calcite veins are preserved [23]. Such veins are regarded to have favored the preservation of oil in the Dongying Depression [24, 25]. However, there is a lack of systematic description and classification of the veins. Further, there is no consensus regarding the genesis of different calcite veins. The formation of calcite veins is linked to the timing of hydrocarbon generation, and fluid overpressure is considered a critical factor for the occurrence of natural fractures in shale [3, 23]. Organic acids and by-products formed during oil generation promote the dissolution of micrite, providing ions for calcite precipitation in veins [3]. Wang et al. [26] suggested that the migration of hydrocarbon-bearing fluids and consequent mineral precipitation led to continuous vein growth and expansion.

In this study, the calcite veins in the Dongying Depression were systematically characterized using petrographic and geochemical methods. The mechanism and fluid sources responsible for vein formation were discussed. The results of this study provide a better understanding of the impact of vein formation on shale oil reservoirs.

2. Geological Setting

The Bohai Bay Basin, located in eastern China, is an important hydrocarbon-producing basin. It comprises several subbasins and covers approximately 200,000 km^2 (Figure 1(a)). The Jiyang Subbasin is one of the subbasins bounded by the Tan-Lu Fault to the east, Chengning Uplift to the northwest, and Luxi Uplift to the south. The study area, i.e., Dongying Depression, is a secondary tectonic unit of the Jiyang Subbasin and has an area of around 5,700 km^2 (Figure 1(b)) [27]. It is situated in the south-eastern part of the Jiyang Subbasin and is bordered by the Luxi Uplift to the south, Guangrao rise to the southeast, Chengjiazhuang rise to the north, and Binxian and Qingcheng rises to the west. The study region comprises the south-western Boxin, central Niuzhuang, north-western Lijing, and north-eastern Minfeng sags and the central diapiric anticline (Figure 1(c)).

The tectonic evolution of the Dongying Depression in the initial syn-rifting stage can be divided into rifting I to IV (Figure 2). During rifting II and III, extensive lacustrine expansion occurred, resulting in a broad semideep lacustrine and deposition of abundant fine-grained sedimentary rocks in the Es4s-Es3x interval [27]. The Dongying Depression is filled with Cenozoic sediments forming six formations, namely, the Paleogene Kongdian (Ek), Shahejie (Es), and Dongying (Ed) Formations; Neogene Guantao (Ng) and Minghuazhen (Nm) Formations; and the Quaternary Pingyuan (Qp) Formation (Figure 2). The Es Formation is divided into four members as Es1, Es2, Es3, and Es4 from the top to the base. The Es4 and Es3 members can be further divided into Es4x, Es4s, Es3x, Es3z, and Es3s from the base to the top.

During the accumulation of the Es4x, sedimentation occurred in a dry and hot climate, and four sags were relatively isolated. The sags subsequently merged into a shallow lake in the Es4s. Under comparatively warm-damp conditions, salt lacustrine facies comprising gypsum, argillaceous carbonate, calcareous mudstone, and shale were deposited (Figure 2) [28]. During the accumulation of the Es3x, the Dongying Depression was intensely faulted. The basement rocks rapidly subsided to form a relatively sustained deep-lacustrine environment with the lacustrine sediments comprising mudstone, calcareous mudstone, and shale. The Es3z and Es3s lithofacies are similar to the Es3x lithofacies and are characterized by stable sedimentation in the lacustrine basin that resulted in calcareous mudstone, shale, etc. (Figure 2) [28]. The interval of interest for this research is Es4s and Es3x, in which calcareous mudstone and shale with many bedding-parallel calcite veins are preserved.

3. Materials and Methods

The Es3x-Es4s interval is penetrated by the NY1 and FY1 wells in the Dongying Depression. A total of 17 core samples were collected from the NY1 and FY1 wells for thin sections (Table 1). Samples with bedding-parallel calcite veins ($n = 9$) were trimmed into cubes and polished. The calcite veins and host rocks were then drilled from the cubes using a microscope-mounted drilling assembly (1 mm diameter drill bit; ×10 magnification). Similarly, samples of micritic carbonate laminae ($n = 8$) were collected and prepared.

Cathodoluminescence (CL) observation of thin sections was performed under a Leica DM2500P CL microscope with a voltage of 12 kV and current of 250 μA. The thin sections were coated by a Pt conducting layer and then observed under a ZEISS S-3400 N field emission scanning electron microscope (SEM) with ETH of 15–20 kV. All the

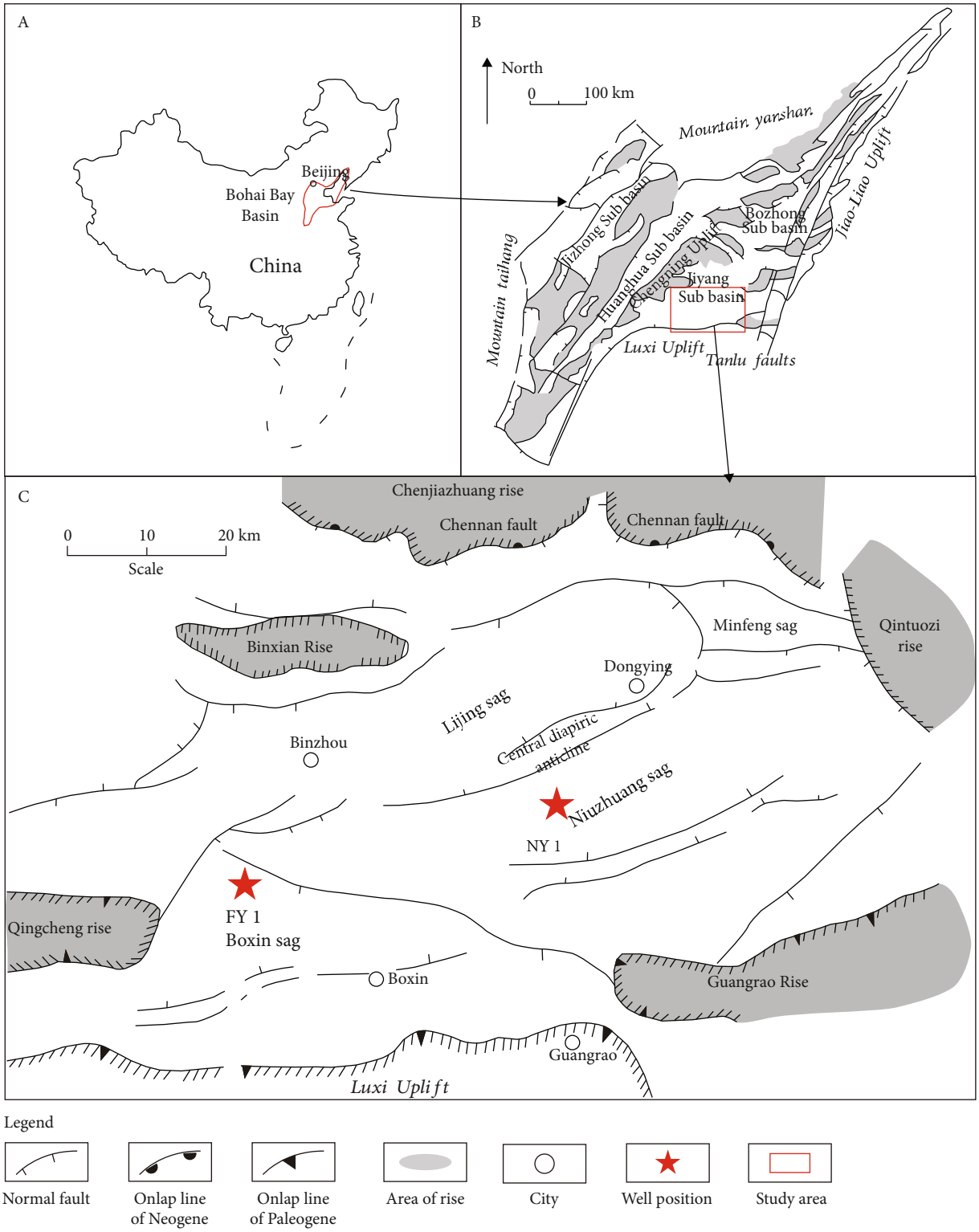

Figure 1: Location and tectonic setting of the Bohai Bay Basin (a, b) and Dongying Depression (c).

microscopic analyses were performed at the State Key Laboratory of Geological Processes and Mineral Resources in Beijing.

An X-ray diffraction (XRD) analysis of the powdered samples was conducted by using a D/max-2500 theta/theta rotating anode X-ray diffractometer. The total organic carbon (TOC) of bulk rocks was determined using a carbon sulfur analyzer, LECO CS600. The measurement technique used here is based on sample combustion in an O_2 atmosphere to convert TOC to CO_2. Thermal maturities were determined

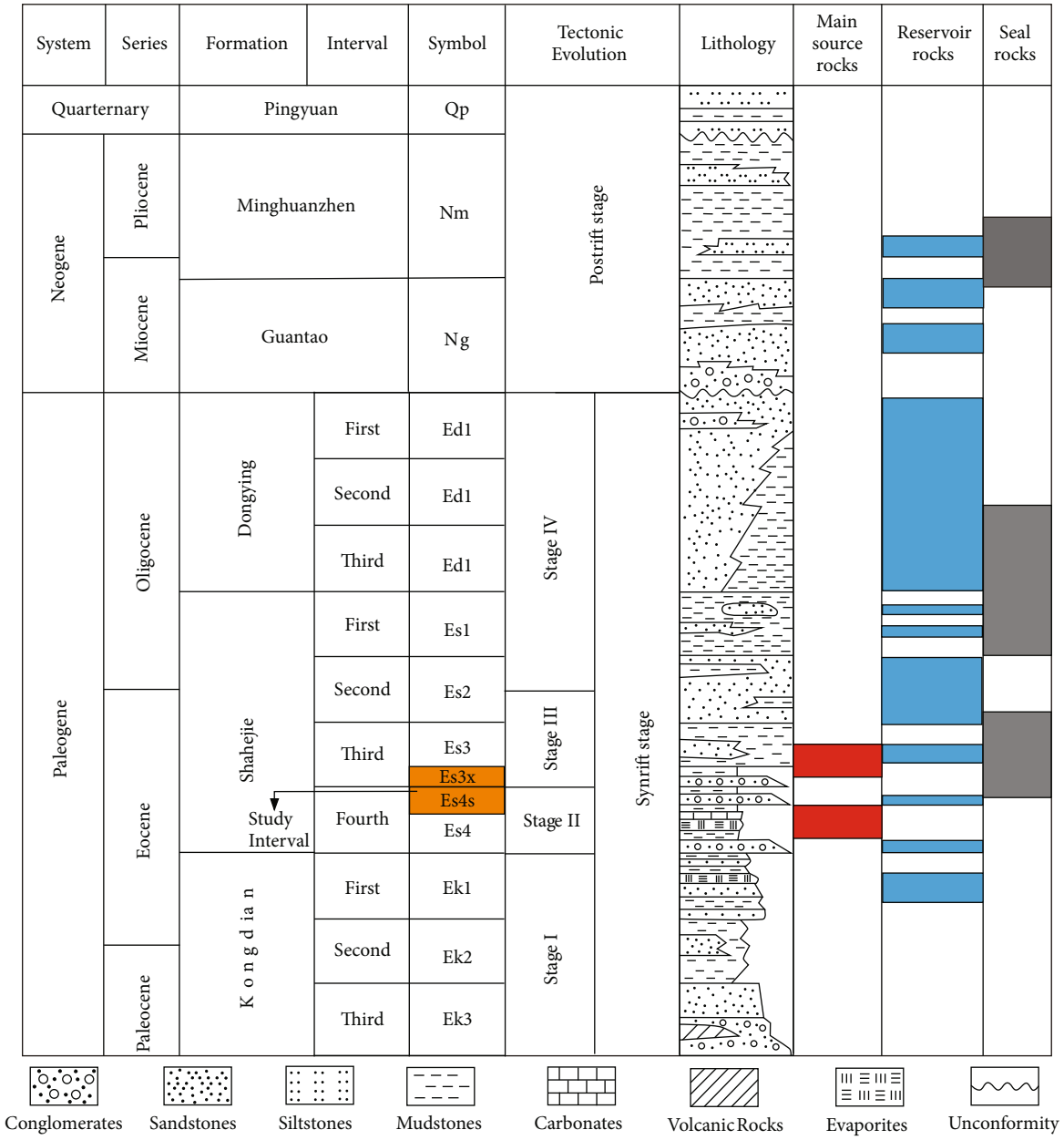

Figure 2: Stratigraphy of the Dongying depression, showing the tectonic and sedimentary evolution stages [29].

Table 1: The depth and description of sample.

Number	Sample	Depth (m)	Description	Number	Sample	Depth (m)	Description
1	NY1-4	3316.00	Fibrous calcite veins	10	FY1-18	3418.47	Fibrous and blocky calcite veins
2	NY1-5	3296.06	Fibrous calcite veins	11	FY1-19	3418.35	Blocky calcite veins
3	NY1-10	3414.23	Fibrous calcite veins	12	FY1-23	3438.52	Fibrous calcite veins
4	NY1-13	3458.57	Blocky calcite veins	13	FY1-28	3196.00	Fibrous calcite veins
5	NY1-1	3331.79	Shale with micritic carbonate	14	FY1-30	3197.27	Fibrous calcite veins
6	NY1-2	3329.30	Shale with micritic carbonate	15	FY1-15	3412.14	Shale with micritic carbonate
7	NY1-3	3330.15	Shale with micritic carbonate	16	FY1-16	3377.05	Shale with micritic carbonate
8	NY1-7	3401.20	Shale with micritic carbonate	17	FY1-17	3378.75	Shale with micritic carbonate
9	NY1-11	3414.56	Shale with micritic carbonate				

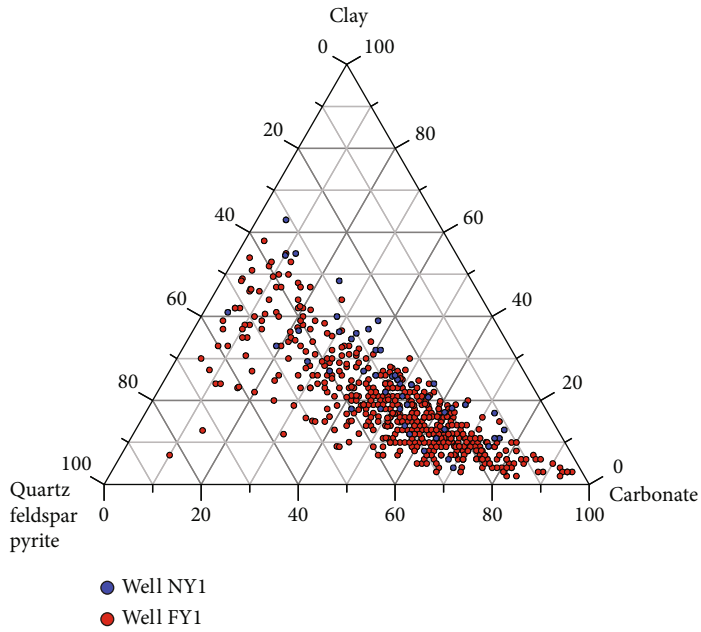

Figure 3: Ternary diagram of the mineral composition of the Shahejie Formation Es4s-Es3x shale.

Table 2: The X-ray diffraction data of samples from well NY1 and FY1 (%).

		NY1 $N = 49$	FY1 $N = 562$
Clay minerals	Avg.	24.1	17.8
	Max	59	57
	Min	4	2
Quartz	Avg.	22.1	24.9
	Max	45	60
	Min	7	2
Feldspar	Avg.	5.0	4.6
	Max	22	35
	Min	1	1
Calcite	Avg.	32.8	38.3
	Max	73	78
	Min	2	1
Dolomite	Avg.	13.3	11.9
	Max	76	93
	Min	1	1

using a Leitz MVP-3 microscope photometer, which helps measure vitrinite reflectance (Ro) values. Asphalt was extracted before pyrolysis. The Rock-Eval parameters measured include the free hydrocarbons (S1), hydrocarbons cracked from kerogen (S2), carbon dioxide relieved from organic matter (S3), and maximum yield temperature of pyrolysate (Tmax). The microanalysis of TOC was conducted using a LECO CS600 at the Laboratory of Geological Microbiology of the China University of Geosciences, Beijing. The microdrilling samples of micritic carbonate laminae, veins, and host rocks were analyzed for trace elements, rare earth elements (REEs), carbon and oxygen isotopes, organic carbon isotopes, and strontium isotopes. These analyses were conducted at the Analytical Laboratory of the Beijing Research Institute of Uranium Geology. Trace elements and REEs were measured using a NexION300D apparatus for inductively coupled plasma-mass spectrometry (ICP-MS; >10 ppm, error < 5%; <10 ppm, error < 10%). Carbon and oxygen isotopes were measured by adding concentrated phosphoric acids to produce the CO_2 which were tested by a MAT-253 gas isotope mass spectrometer. Carbon and oxygen isotope compositions are reported in the standard delta notation as permil (‰) relative to Vienna Pee Dee Belemnite (VPDB), with an analytical precision of ±0.2‰ for carbon isotopes and ±0.1‰ for oxygen isotopes. Organic carbon isotope was measured using a MAT-253 gas isotope mass spectrometer when burning a sample in flowing oxygen to produce the CO_2. Strontium isotope was determined by using a phoenix thermal ionization mass spectrometer (TIMS). The powder samples (0.1 to 0.5 g) were digested in 5 mL HF and 2 mL $HClO_4$. Strontium was separated in 5 mL HCl using 200 to 400 mesh cation exchange resin. During mass spectrometry measurement, the Sr isotope ratio was obtained at the 1250 ± 50°C and an ion current intensity of 1×10^{-11} A in vacuum. The $^{87}Sr/^{86}Sr$ ratio was corrected for mass fractionation using $^{88}Sr/^{86}Sr = 8.37521$.

4. Results

4.1. Petrologic Features. Observations at NY1 and FY1 wells suggest that the lithologies of Es4s and Es3x mainly consist of calcareous mudstone and shale, sandy mudstone, gypsum mudstone, and argillaceous limestone [25]. The carbonate minerals are interbedded in the mudstone or shale and occur

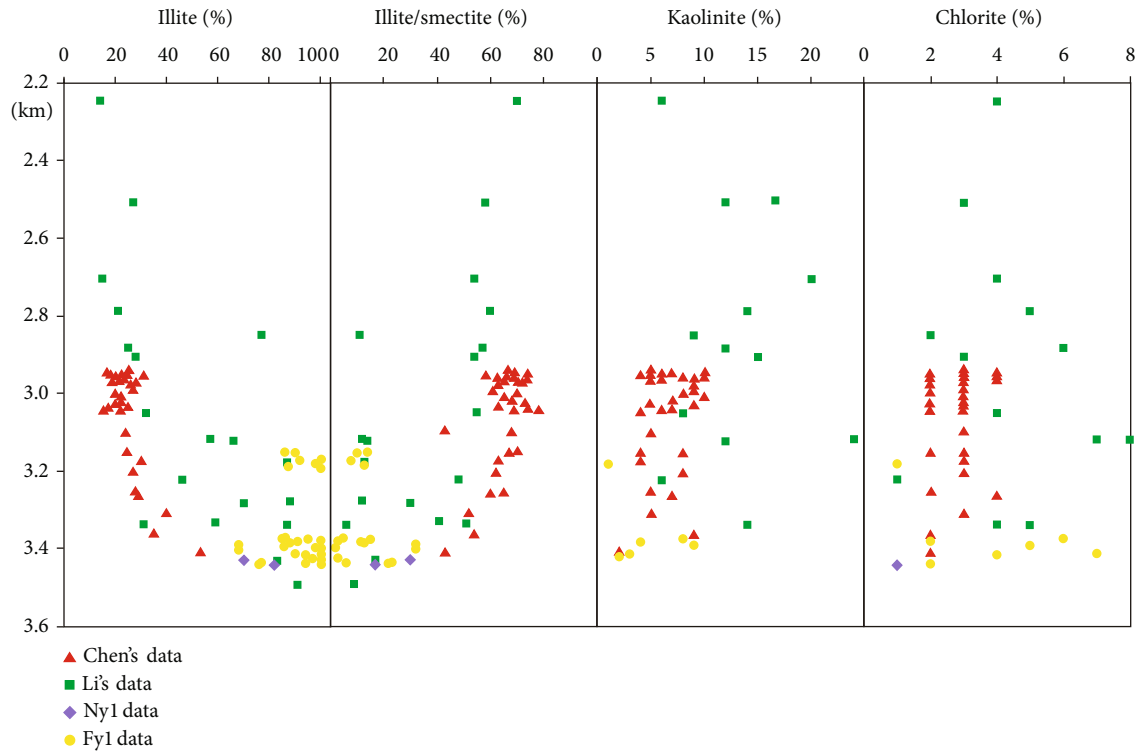

Figure 4: Proportions of clay minerals in samples from Es3 to Es4. Data are from the NY1 and FY1 wells; the data were collected for this study and from some previously published work on the study area [30, 31].

as primary micritic carbonate lamina, and secondary carbonate vein fills according to their morphology and contact relationship with the neighboring layers.

4.1.1. Mineral Composition. The XRD analysis of the bulk samples indicates that the mineral compositions include quartz, feldspar, carbonate, clay minerals, pyrite, minimum barite, and anhydrite. The average content of the main minerals (clay, quartz, feldspar, and carbonate) of NY1 and FY1 wells is shown in Figure 3. Collectively, they account for more than 90% of the bulk samples. The data of clay (Table 2) show that the content in the NY1 well ranges from 4% to 59%, with an average of 24.1%. The average feldspar and quartz contents are 5% and 22.1%, respectively. The average calcite and dolomite contents are 32.8% and 13.3%, respectively. The clay mineral content in the FY1 well ranges from 2% to 57%, with an average of 17.8%. The average feldspar and quartz contents are 4.6% and 24.9%, respectively. The average calcite and dolomite contents are 38.3% and 11.9%, respectively.

Statistical analysis of the clay mineral content of the NY1 and FY1 wells and some previously published data from the study area indicate that the clay minerals include kaolinite, mixed illite/smectite, illite, and chlorite (Figure 4) [30, 31]. The illite content increases significantly with increasing depth, whereas the mixed illite/smectite content shows the opposite trend. The kaolinite content also displays a negative correlation with the depth. The chlorite content is less than 8%.

4.1.2. Microstructure of Calcite Veins. Bedding-parallel calcite veins are widely developed in calcareous shale and are brighter in color than the host rocks in cores. These veins also vary in size and range from about 1-10 mm in thickness and 3-100 mm in length (but they are limited by the size of the cores) (Figure 5). The surfaces of the calcite veins are smooth, but it is difficult to distinguish the types of veins from the cores. The veins are lenticular and lamellar and show the characteristics of horizontal and vertical extension. The bedding-parallel calcite veins consist of several overlapping lenses and laminae (Figures 5(a) and 5(f)) that often contain solid inclusions. Bedding-parallel fractures with a thickness of approximately 1 mm thick were found near the calcite veins (Figures 5(b) and 5(c)).

In the thin sections, antitaxial and syntaxial veins can be distinguished. Antitaxial calcite veins typically contain fibrous crystals with high length/width ratios and are almost perpendicular to the host rocks. The fiber boundaries are smooth (Figures 6(a) and 6(b)). The bedding-parallel calcite veins consist of several small veins with lensoid and lamellar shapes and comprise various solid inclusions of host rock debris. Some inclusions are banded parallel to the vein-wall interface (Figures 6(c) and 6(d)). Others are locally folded within the veins and arranged as sinusoidal inclusions (Figure 6(b)). The median zone or median line consists of micritic carbonate, usually on one side of the vein (Figures 6(c) and 6(d); Figure 7(a)). Some antitaxial veins do not have a median zone, and the fibers are elongated from one wall to another at high length/width ratios (Figure 6(a)).

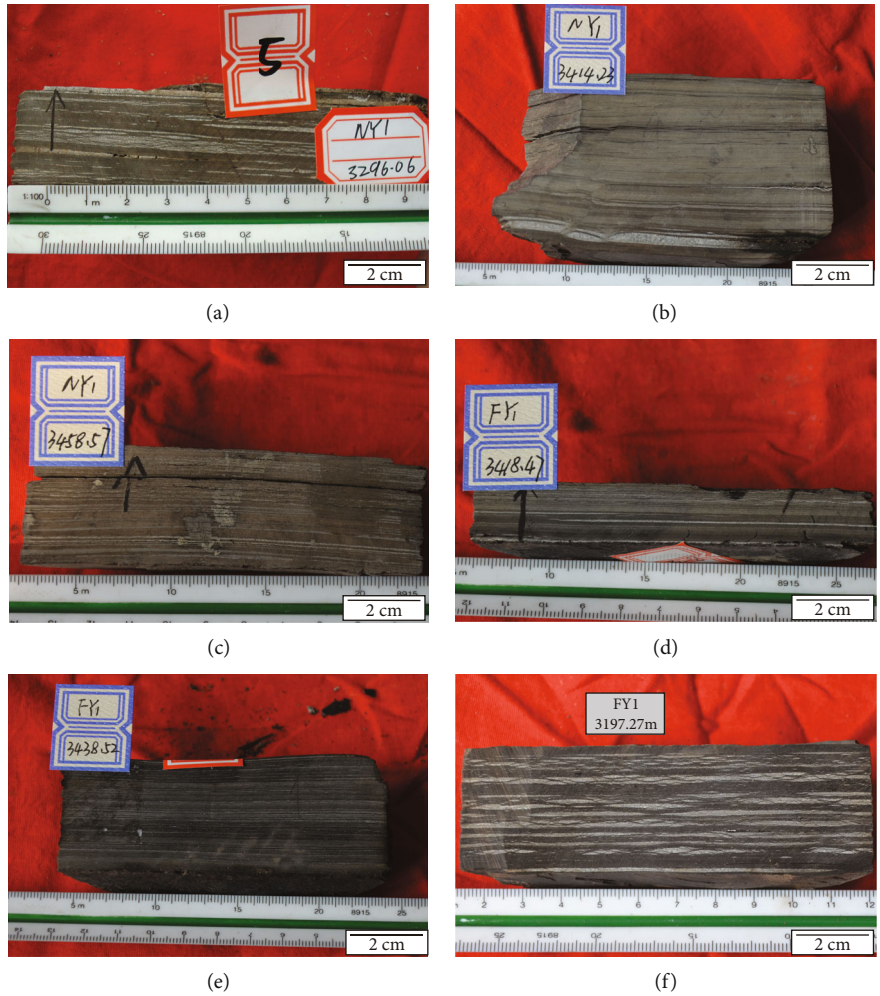

Figure 5: Features of the calcite vein as seen in the core. (a) NY1, 3296.06 m: the bedding-parallel calcite vein consists of a few lenticular and lamellar calcite veins. (b) NY1, 3414.23 m: the calcite vein is approximately 5 mm thick, and fractures have developed in the host rock. (c) NY1, 3458.57 m: the vein is only approximately 1 mm thick, and interbedded shale consists of clay mineral laminae and calcite laminae. (d) FY1, 3418.47 m: this sample is similar to the sample (c) and contains a horizontal fracture at the interface between the vein and host rock. (e) FY1, 3438.52 m: the thickness of vein is less than 1 mm. (f) FY1, 3197.27 m: several lenticular veins overlap to form a bedding-parallel calcite vein and solid inclusions are trapped in it.

In the CL analysis, antitaxial veins with fibrous crystals exhibit a bright red and dully red luminescence (Figure 7(a)). The edge of the lensoid calcite veins exhibit slightly brighter luminescence (Figure 7(b)).

Syntaxial calcite veins contain crystals with coarse-crystalline, blocky morphologies. The contact surface of the vein and host rock is smooth. The crystal size varies from several to a hundred microns. The dark solid inclusions often fill between the blocky crystal, creating irregular shapes (Figures 6(e), 6(g), and 6(h)). The syntaxial veins with blocky crystals show oscillatory CL zoning with the exterior of crystals being brighter than the interior. In addition, fibrous calcite veins are observed near the blocky calcite veins, ranging in size from tens to hundreds of microns (Figures 6(f) and 6(h)) and showing a brighter red luminescence than the median zone of the blocky calcite vein (Figures 7(c) and 7(d)).

Almost all the veins are somewhat fluorescent. The antitaxial calcite veins with fibrous crystals show the most intense green to dark-green coloring (Figures 8(b) and 8(c)). However, the blocky crystals and micritic carbonates in the central zone of the antitaxial calcite veins are less fluorescent than their host rock and the fibrous calcite within the same sample (Figures 8(d) and 8(e)). Syntaxial calcite veins with blocky crystals exhibit comparatively weak fluorescence (Figure 8(a)).

4.1.3. Calcite Veins. The solid inclusions in fibrous and blocky calcite veins were identified as clay minerals, quartz, pyrite framboids, and organic matter (OM) by SEM (Figure 9). The pyrites are widely distributed in the shale and the solid inclusions between lenticular calcite veins (Figures 9(c) and 9(d)) and are also present in the center of the veins (Figure 9(b)). OM is distributed along

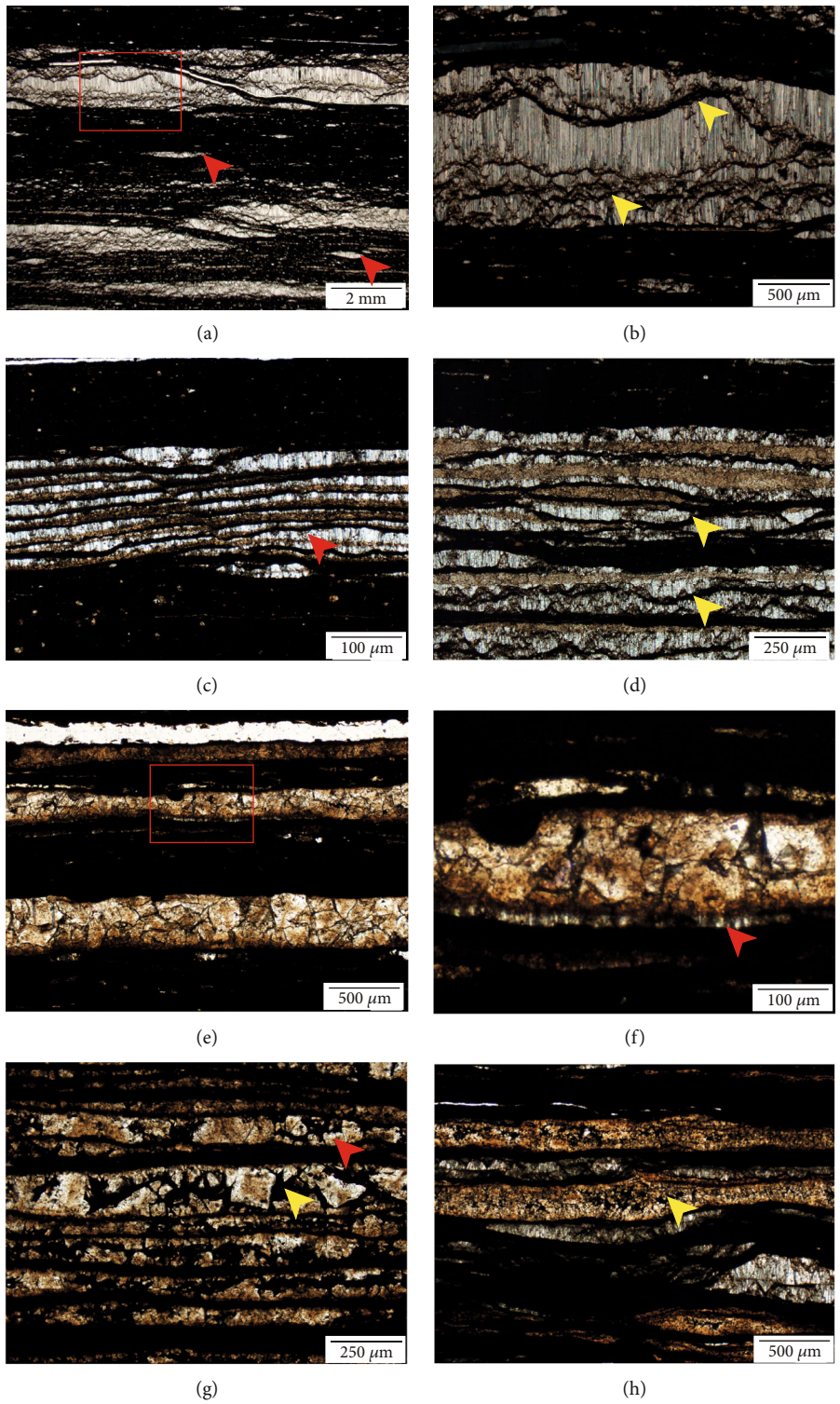

Figure 6: Calcite veins seen under a microscope. (a) FY1, 3197.27 m: a calcite vein with fibrous crystals, with many small calcite lenses (red arrows) possibly growing in host rock and solid inclusions (yellow arrows) arranged in a sinusoidal manner and as inclusion trails. (b) The red outline of (a). (c) NY1, 3414.23 m: sample shows coexistent initial micritic carbonate and fibrous calcite. Fibrous calcite grows on the flanks of micritic carbonate (red arrow). (d) FY1, 3438.52 m: the sample is similar to sample (c) with abundant solid inclusions (yellow arrows). (e) NY1, 3458.57 m: calcite veins consisting of blocky crystals with single crystals about 100 μm. (f) The red outline of (e), in which fibrous calcite are seen near the blocky crystals (less than 40 μm, red arrow). (g) FY1, 3418.35 m: the calcite veins consist of blocky crystals (red arrow), but the sizes of the single crystals are obviously different, with solid inclusions (yellow arrow) filled between these crystals. (h) FY1, 3418.47 m: fibrous calcite veins and coarse-grained carbonate veins grow together. The dark materials are filled between the coarse-grained carbonates (yellow arrow).

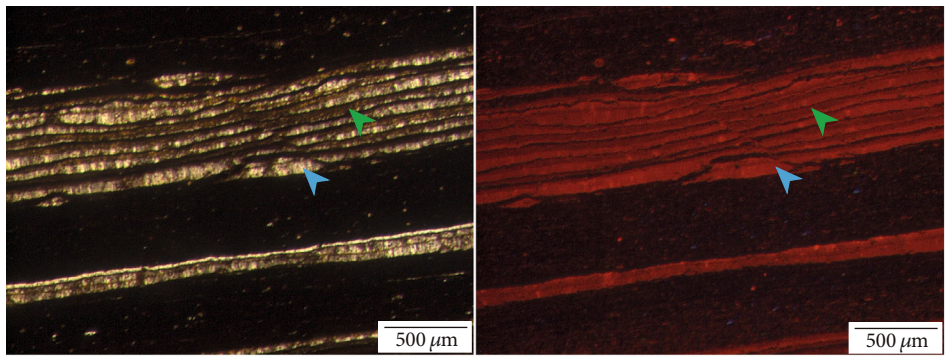

(a)

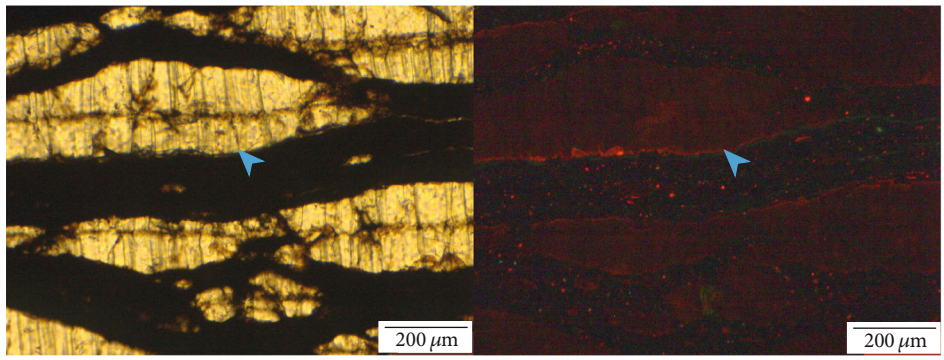

(b)

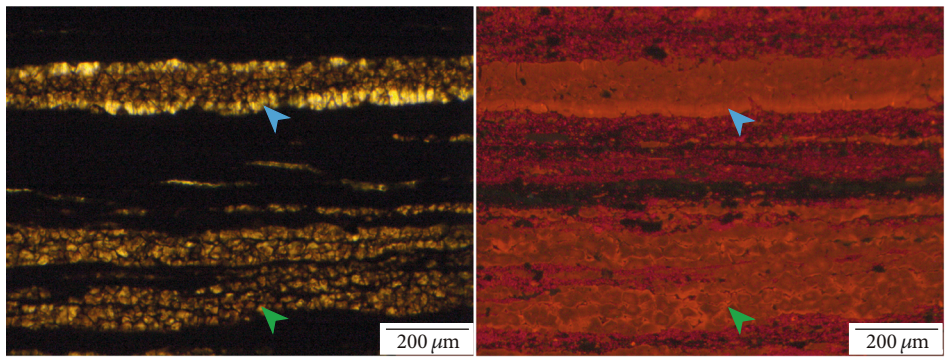

(c)

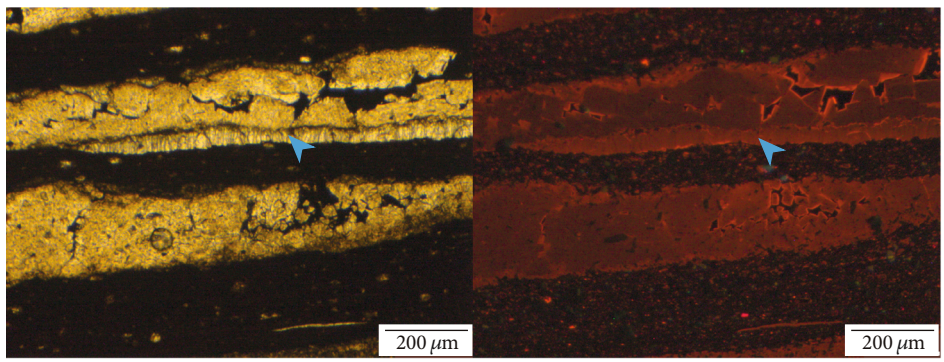

(d)

Figure 7: Calcite veins under a cathodoluminescence (CL) microscope. (a) NY1, 3414.23 m: the micritic carbonates are in the median zone (green arrow) flanked with fibrous crystals (blue arrow) or towards one side of the vein. Fibrous calcite crystals with brighter red luminescence contrast to the median zone. (b) NY1, 3296.06 m: fibrous calcite crystals show dark luminescence, but the edge of the vein is brighter (blue arrow). (c) NY1, 3458.57 m: blocky crystals have oscillatory zoning (green arrow), and the edge of the fibrous crystals have brighter luminescence (blue arrow). (d) FY1, 3418.35 m: fibrous calcite shows brighter luminescence (blue arrow).

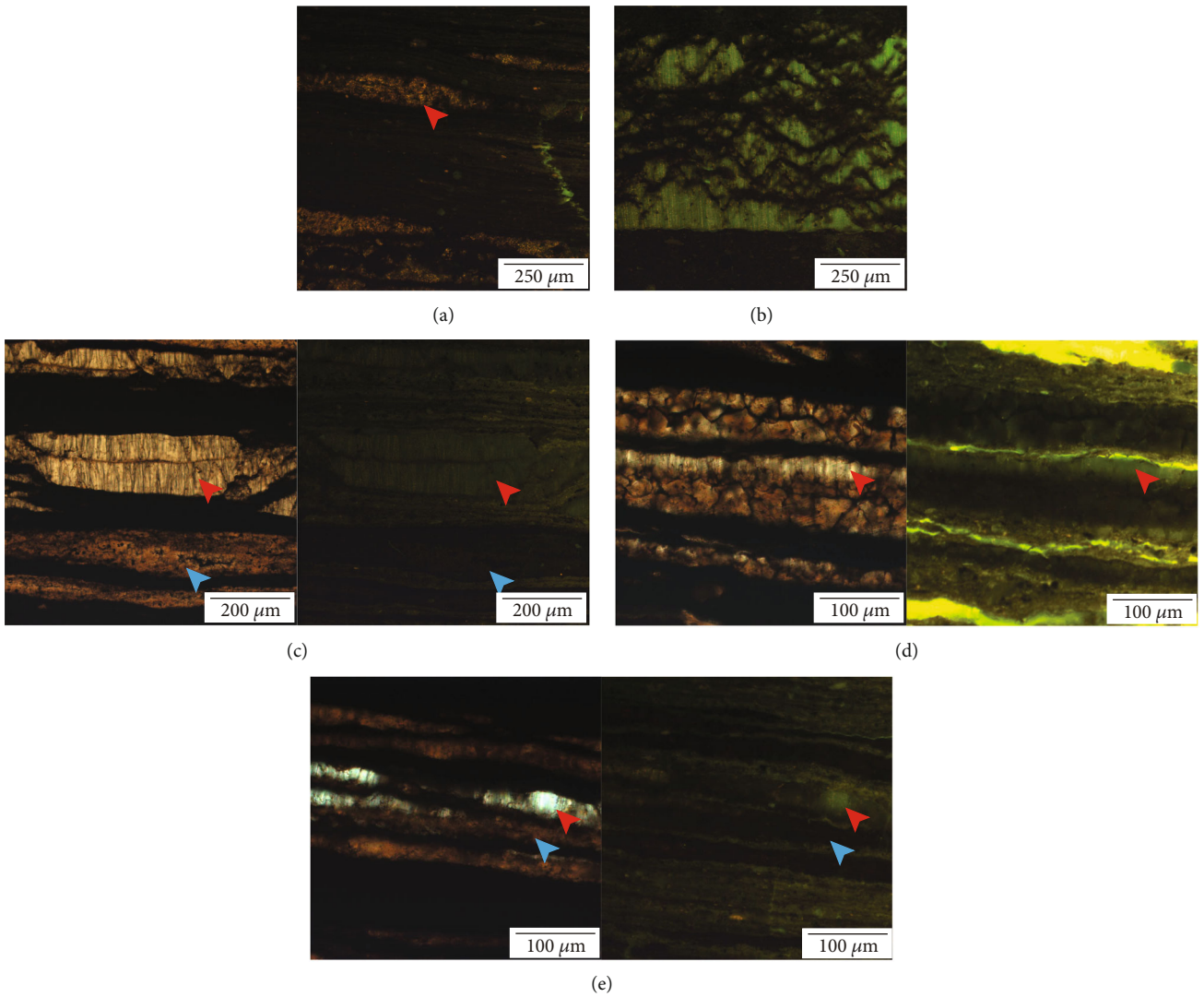

Figure 8: Calcite veins observed under the fluorescence microscope. (a) FY1, 3418.35 m: blocky calcite crystals with weak fluorescence (red arrow). (b) FY1, 3197.27 m: fibrous calcite crystals had the most obvious green fluorescence. (c) FY1, 3418.35 m: fibrous calcite veins are fluorescent (red arrow), and coarse-grained calcite veins are not (blue arrow). (d) NY1, 3458.57 m: blocky crystals in the median zone of the antitaxial calcite veins are less fluorescent than the fibrous calcite with which it coexists and which has greenish fluorescence (red arrow). (e) FY1, 3438.52 m: the sample is similar to sample (d). The micritic carbonate of the median zone is not fluorescent (blue arrow), which is in contrast to the fluorescence of the fibrous calcite (red arrow).

the margin of calcite veins and solid inclusions (Figure 9(h)) and among irregularly shaped blocky crystals (Figure 9(a)). Barite and strontianite can be observed by a qualitative analysis by SEM-energy dispersive X-ray spectroscopy (EDS). Barites can be observed at the margin of fibrous calcite veins and are partially replaced by calcite (Figure 9(e)). Strontianites have irregular shapes and fill in calcite veins (Figures 9(g)) and are very common in the fibrous calcite vein.

4.2. Organic Matter. The TOC contents of the bulk rock in the NY1 (188 samples) and FY1 (143 samples) wells are 0.15–9.32 wt. % and 0.11–9.05 wt. %, respectively, with average values of 3.00 wt. % and 2.41 wt. %, respectively. Samples with TOC greater than 1 wt. % account for 93.8% and 98.5% of the total samples analyzed from NY1 and FY1 well, respectively. The S1 + S2 values of the bulk samples are approximately 15 mg/g. The plot of HI versus the pyrolysis Tmax indicates principally type I kerogen [27]. The vitrinite reflectance (Ro) values for NY1 and FY1 are 0.52–0.80% and 0.51–0.91%, respectively (Figure 10). Results of the microanalysis of the TOC content of the host rock are listed in Table 3; the TOC content ranges from 5.72 to 15.20 wt. %.

4.3. Geochemistry. The $\delta^{18}O$ values of the host rock of the fibrous calcite vein range from -11.3‰ to -10.4‰. The fibrous calcite veins are depleted by about 1.6‰ relative to the host rock and decrease from -13.2‰ to -11.9‰. The host rocks with the blocky calcite veins have a broad range of $\delta^{18}O$ values from -10.9‰ to -8.9‰. The $\delta^{18}O$ values in blocky

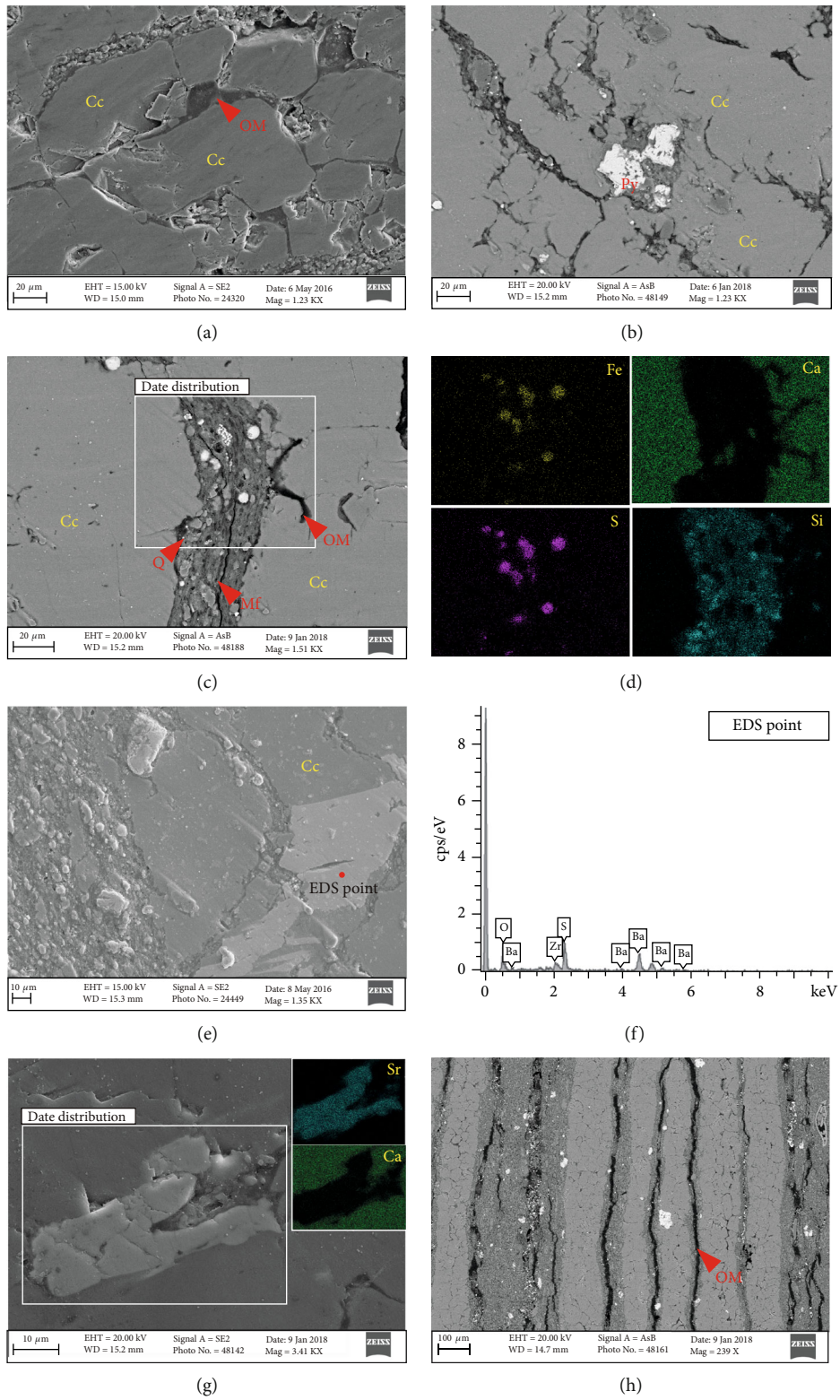

Figure 9: Calcite veins observed under the scanning electron microscope. (a) NY1, 3458.57 m: the spaces between blocky calcite crystals are filled with clay minerals and OM. (b) FY1, 3197.27 m: pyrite is packed in the fibrous calcite. (c, d) NY1, 3296.06 m: solid inclusions are present, and the microfracture (Mf) is subparallel to the calcite vein. The energy dispersive X-ray spectroscopy (EDS) image shows the mineral composition of the solid inclusion. Pyrite framboids, quartz grains, and OM are present on the margin of the calcite vein. (e, f) FY1, 3413.44 m: barite appears in the fibrous calcite veins. (g) FY1, 3197.27 m: strontianite appears in the fibrous calcite veins. (h) NY1, 3458.57 m: bedding-parallel calcite veins have blocky crystals. Between these veins are solid inclusions associated with clay minerals and OM. Cc: calcite; Py: pyrite: Q: quartz; Mf: microfracture; OM: organic matter.

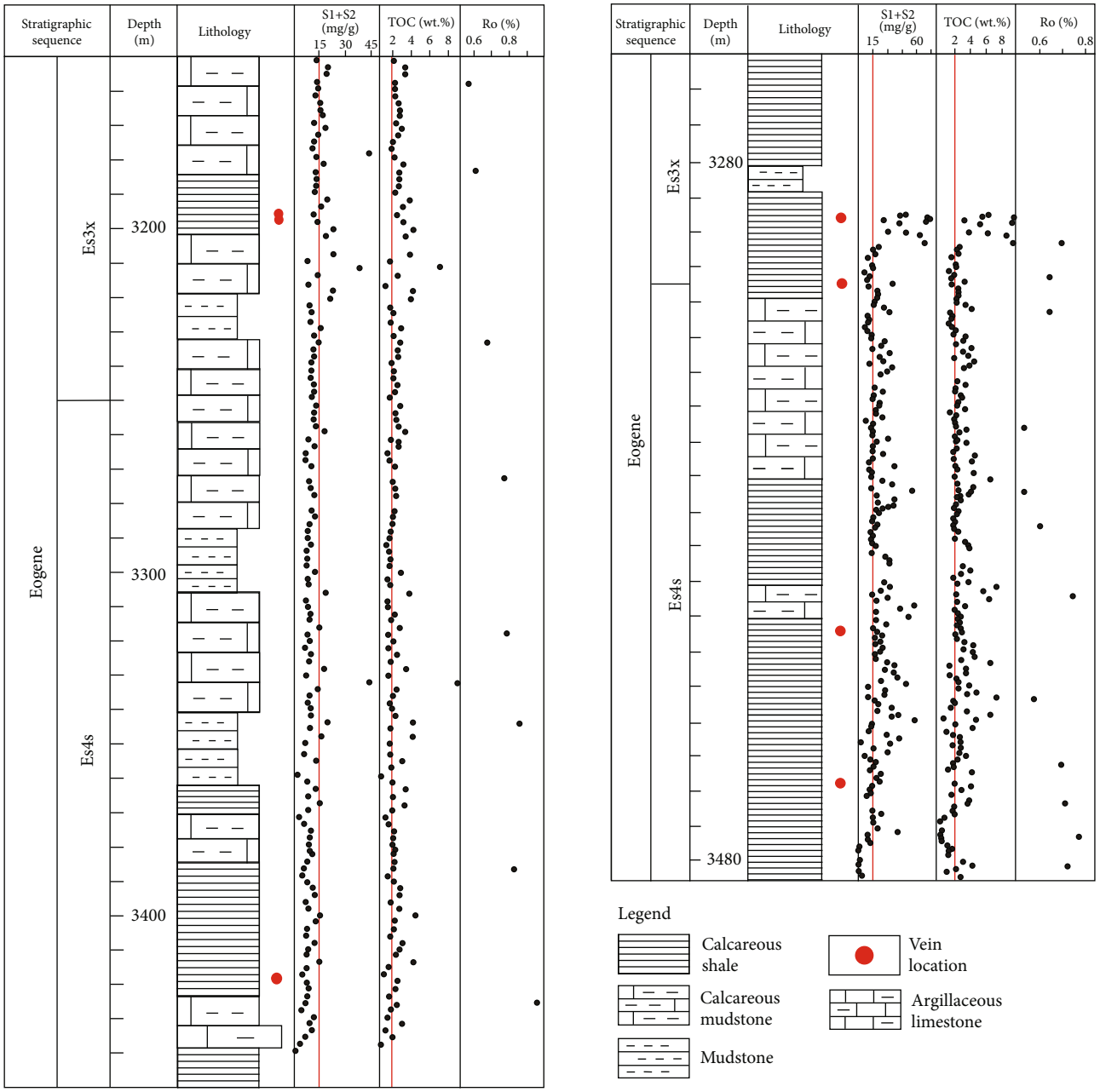

Figure 10: Location lithology and geochemical characteristics of samples FY1 and NY1.

calcite veins are -11.6‰ and -8.9‰. The $\delta^{18}O$ values of micritic carbonate laminae range from -11.5‰ to -8.4‰, with an average of -9.5‰ (Table 4).

The measured $\delta^{13}C$ values for host rocks with fibrous calcite veins range from -0.4‰ to 2.6‰. The $\delta^{13}C$ values of fibrous calcite veins range from 2.8‰ to 4.3‰. The $\delta^{13}C$ values of the host rocks with blocky calcite veins are -1.1‰ and 1.8‰. The $\delta^{13}C$ values of the blocky calcite veins are 0.2‰ and 3.4‰. The $\delta^{13}C$ values of micritic carbonate laminae range from 2.1‰ to 4.8‰, with an average of 3.5‰. The $\delta^{13}C_{org}$ values of fibrous calcite veins range from -24.6‰ to -22.9‰, averaging -23.7‰, whereas those of their host rocks range from -24.2‰ to -22.3‰. The $\delta^{13}C_{org}$ values of blocky calcite veins are -27.2‰ and -27.3‰, whereas those of their host rocks are -27.0‰ and -27.4‰, respectively.

The Sr isotopic compositions of fibrous calcite veins, blocky calcite veins, and host rocks are in the ranges from 0.710572 to 0.710812, 0.710869 to 0.710970, and 0.710729 to 0.711335, respectively. The Sr isotopic composition of micritic carbonate laminae ranges from 0.710449 to 0.710930, with an average value of 0.710718.

The data of trace elements and REEs for fibrous calcite veins, blocky calcite veins, host rocks, and micritic laminae are listed in Tables 5–7.

Table 3: The data of microanalysis of total organic carbon (TOC) of the host rock.

Sample	Depth (m)	TOC (wt. %)	Sample	Depth (m)	TOC (wt. %)
NY1-4	3316.00	11.50	NY1-13	3458.57	6.83
NY1-5	3296.06	12.40	FY1-19	3418.35	5.72
NY1-10	3414.23	8.35	FY1-28	3196.00	15.20
NY1-10	3414.56	7.10	FY1-30	3197.27	10.20
NY1-13	3458.60	7.82			

5. Discussion

5.1. Formation Mechanism of Fractures. Fractures provide the space for the precipitation of calcite in the veins and are thereby preconditions for the formation of the latter. The calcite veins normally show bedding-parallel features. This indicates that the internal stress of shale, rather than external stress (tectonic activity) [32, 33], is the main factor that the precipitation of the calcite vein is accommodated. The presence of OM in the calcite veins indicates that hydrocarbon-bearing fluids flowed through the veins and filled them since vein opening. The rocks in the NY1 and FY1 wells are characterized by the high carbonate content, low feldspar content, and a TOC of almost more than 2 wt. %. Moreover, the rocks are in the oil window (Ro > 0.5%) and have good hydrocarbon potential (type I kerogen and high S1 + S2 values) (Figure 3; Figure 10). Wang et al. [26] reported that the fluid inclusions in calcite veins normally have yellow to blue-green colors under ultra-violet (UV) illumination. The trapping temperature exceeded 70°C because of the homogenization temperatures of inclusions. Thus, the thermal evolution of the OM probably generated the acidic fluids that dissolved the carbonate in the rocks. Previous research has also suggested that the fluids were generated as the OM became matured, resulting in an increase in the local volume with abnormal overpressure within the Es3 and Es4 intervals, rather than by disequilibrium compaction [27]. In addition, with increasing burial depth, the mixed illite/smectite content decreases, and it transforms into illite (Figure 4). The dehydration of clay minerals causes structural modifications, such as the opening of pores and/or horizontal fractures (Figure 9(c)) [34], which are likely responsible for the fluid overpressure [26]. The fibrous crystals that grow almost perpendicular to the fracture wall of host rocks and have smooth fiber boundaries indicate that overpressure is not likely caused by horizontal compression. According to morphology changes with respect to the wall of fibrous calcite cemented veins, Rodrigues et al. [18] identified the opening of veins owing to horizontal compression, which shows an obvious angle change from inner zones to outer zones in the fibrous calcite. Since the shear stresses acted at the vein margins, the previously consolidated vein resisted shortening, whereas the host rock did not. Thus, the calcite veins formed by horizontal compression are expected to curve with respect to the wall; however, such curved veins are not present in our samples (Figures 6(a) and 6(c)).

Changes in lithology during sediment accumulation are another potential factor for the formation of bedding-parallel fractures. The main changes are a result of the growth of micritic carbonates in the median zone, with flanking fibrous crystals, or the growth of fibrous crystals at the margin of the blocky vein (Figures 6(c), 6(d), and 6(f)). The major rocks in the Es4s-Es3x intervals are laminated organic-rich shale, consisting of micritic and clay laminae [25]. Interlayer fractures often grow at the interface between micritic and clay laminae [34, 35]. This is because the transitional surface is the weakest zone in the rock, allowing for fracturing by fluid pressure. Therefore, the secondary fractures promote the migration of hydrocarbon-bearing fluids and the consequent calcite precipitation.

In summary, given increasing depth, OM can generate acidic fluids that dissolve carbonate minerals, and the mixed illite/smectite is transformed to illite, thereby promoting the formation of spaces and fluid overpressure. Besides, fluid overpressure has a vital impact on forming bedding-parallel fractures in the transitional surface of the rock and interlayer within rocks.

5.2. Source of Vein Fill. The increase in pore pressure may affect the chemical equilibrium of the aqueous system by increasing the solubility of carbonate minerals [5]. The OM is thermally mature. Thus, it expels organic acids and large volumes of CO_2 [36], leading to the dissolution of the primary carbonate in the host rock. As the pore pressure increases, an increasing amount of $CaCO_3$ is dissolved into fluids until the maximum is reached [37]. However, as the pore pressure decreases drastically because of horizontal microfracturing and pore opening, the supersaturated pore fluid causes carbonate precipitation in the fracture system. Both strontianite and barite observed within the calcite veins indicate that they precipitated simultaneously with the calcite. Strontianite is a rare low-temperature hydrothermal mineral. Unlike strontianite, barite has multiple origins and could form through biogenic and hydrothermal processes [38–40]. The coexistence of strontianite and barite indicates the possible influence of magmatic hydrothermal fluid [39].

5.2.1. Trace Elements and Rare Earth Elements (REEs). Data of trace elements and REEs can potentially offer information on the source of minerals in veins and the fluid pathways [7]. Chondrite-normalized REEs of micritic laminae, fibrous and blocky calcite, and host rocks show similar patterns (Figure 11). The δEu values for the micritic laminae and host rocks are similar to those from most of the calcite veins. The NY1-10 dataset has an anomalous δEu value of 1.57, which may be associated with the preferential leaching of Eu-rich material (for example, feldspar), reductive vein formation conditions, or transformation into divalent Eu as temperature increases [41]. The crystal shape of the calcite (fibrous and blocky) in the veins cannot be explained by the REE data

Table 4: The data of $\delta^{13}C_{carb}$, $\delta^{18}O$, $\delta^{13}C_{org}$, and $^{87}Sr/^{86}Sr$.

	Vein					Host rock					Micrite				
	$\delta^{13}C_{carb}$ (‰)	$\delta^{18}O$ (‰)	$\delta^{13}C_{org}$ (‰)	$^{87}Sr/^{86}Sr$	Err.	$\delta^{13}C_{carb}$ (‰)	$\delta^{18}O$ (‰)	$\delta^{13}C_{org}$ (‰)	$^{87}Sr/^{86}Sr$	Err.		$\delta^{13}C_{carb}$ (‰)	$\delta^{18}O$ (‰)	$^{87}Sr/^{86}Sr$	Err.
NY1-4	2.8	-12.7	-24.5	0.710766	0.000011	1.5	-11.3	-24.2	0.711335	0.000013	NY1-1	2.6	-8.7	0.710449	0.000013
NY1-5	3.9	-13.2	-23.3	0.710690	0.000011	-0.4	-11.1	-23.4	0.711281	0.000012	NY1-2	3.4	-8.8	0.710525	0.000013
NY1-10	4.3	-12.3	-24.6	0.710812	0.000015	0.6	-10.4	-24.2	0.711259	0.000015	NY1-3	2.1	-8.9	0.710587	0.000022
FY1-28	4.2	-13.0	-22.9	0.710616	0.000017	2.2	-11.1	-22.3	0.711265	0.000018	NY1-7	4.3	-8.4	0.710930	0.000016
FY1-30	3.9	-11.9	-23.0	0.710572	0.000018	2.6	-11.3	-22.8	0.710729	0.000014	NY1-11	3.3	-8.6	0.710905	0.000014
AVG.	3.8	-12.6	-23.7	0.710691		1.3	-11.0	-23.4	0.711174		FY1-15	3.2	-11.5	0.710756	0.000016
NY1-13	0.2	-8.9	-27.2	0.710970	0.000011	-1.1	-8.9	-27	0.711221	0.000016	FY1-16	4.8	-11.4	0.710861	0.000009
FY1-19	3.4	-11.6	-27.3	0.710869	0.000014	1.8	-10.9	-27.4	0.711015	0.000011	FY1-17	4.1	-9.6	0.710729	0.000018
											AVG.	3.5	-9.5	0.710718	

Table 5: The trace elements results of veins, host rocks, and micritic lamina (μg/g).

Sample		Li	Sc	V	Cr	Co	Cu	Zn	Ga	Rb	Sr	Y	Cs	Ba	Pb	Th	U	Ta	Zr	Sr/Ba
NY1-4	Vein	22.9	7.64	66.3	51.1	15.6	30.3	57.0	9.31	47.6	2056	18.0	3.59	317	14.2	4.69	3.42	0.324	34.1	6.5
	Host rock	40.1	12.3	116	79.1	24	50.5	97.2	16.8	84.6	731	18.7	6.29	525	24.6	8.0	5.19	0.599	55.0	1.4
NY1-5	Vein	20.1	7.13	61.6	41.4	9.59	20.0	32.6	7.85	41.1	3610	15.9	3.35	363	8.75	4.24	2.33	0.277	35.4	9.9
	Host rock	50.2	12.5	135	92.5	19.8	47.7	150	18.7	98.6	884	14.3	8.42	524	21.9	8.48	3.44	0.606	60.2	1.7
NY1-10	Vein	7.95	2.34	29.5	18.0	6.47	10.0	15.5	2.95	16.3	4288	4.13	1.24	693	4.51	1.72	1.01	0.102	8.56	6.2
	Host rock	40.8	10.9	116	74.1	36.1	52.6	79.4	14.1	80.4	1846	16.7	6.3	301	19.9	7.37	3.61	0.482	34.7	6.1
NY1-13	Vein	23.5	4.6	46.3	29.4	13.5	20.3	35.4	5.51	30.9	4261	10.1	2.61	361	7.98	3.24	2.84	0.203	11.5	11.8
	Host rock	53.1	9.05	89.0	64.3	25.8	50.8	70.0	14.5	80	1428	15.6	6.97	189	19.8	7.86	4.5	0.569	56.9	7.6
FY1-19	Vein	21.5	5.06	56.9	33.1	114	33.7	38.1	6.48	34.3	8353	9.3	2.94	829	10.1	3.61	2.63	0.241	20.1	10.1
	Host rock	53.5	11.0	128	70.5	28.2	61	112	17.6	94.4	2703	18.2	8.10	281	22.8	8.17	3.87	0.444	31.5	9.6
FY1-28	Vein	22.6	6.38	80.3	42.5	23.3	29.2	30.2	6.6	36.5	2768	12.0	2.92	10456	11.7	3.85	2.88	0.277	30.5	0.3
	Host rock	53.9	12	132	70.5	28.6	62.6	103	17.9	95	2708	21.2	8.19	304	21.5	9.0	5.2	0.609	67.0	8.9
FY1-30	Vein	17.6	8.69	64.6	46.4	15.1	23.4	39.6	7.6	34.4	8552	13.2	2.86	485	9.7	3.1	2.09	0.233	23.6	17.6
	Host rock	26.8	13.1	101	69	19.7	35.9	61.9	11.5	52	2688	18.1	4.32	464	16.3	5.19	3.2	0.389	32.5	5.8
NY1-1		23.9	8.24	82.3	46.5	17.3	37.5	53	8.87	44.6	1653	13.5	3.45	616	18.3	4.93	2.87	0.339	36.7	2.7
NY1-2		23.4	7.25	77	57.4	11.7	21.7	48.2	8.5	39.7	1543	10.7	2.94	628	9.03	4.03	2.26	0.298	27.9	2.5
NY1-3		38.5	10.4	83.8	76.4	15.7	28.3	75.6	16.7	86.6	1149	16.3	6.87	640	11.9	8.62	3	0.621	44.8	1.8
NY1-7		24.3	6.55	62.8	36.7	26.9	19.3	31.7	7.68	40.4	1857	11.4	3.26	430	9.05	4.49	3.77	0.291	28.3	4.3
NY1-11	Micritic lamina	42.1	9.52	108	65.5	21.2	42.3	64.1	15.2	86.8	1162	14.9	6.54	347	23.3	7.48	3.32	0.524	32.9	3.3
FY1-15		32.3	10.3	75.3	59.2	14.2	31.9	27.7	9.75	48.1	3852	17.7	3.73	169	13.8	5.19	3.84	0.35	38.6	22.8
FY1-16		20.1	6.74	65.6	42.9	12.7	31.1	31.9	6.14	31.2	3951	12	2.24	500	7.14	3.3	2.22	0.203	17.9	7.9
FY1-17		20.8	14.6	35.8	42.8	17.7	12.4	40.8	3.96	17.9	2468	17.3	1.26	665	6.58	2.24	1.12	0.144	20.5	3.7
UCC		20	11	60	35	10	20	71	17	112	350	22	3.7	550	20	10.7	2.8	2.2	190	

UCC: upper crust continent based on Taylor and McLennan, 1995 [65].

Table 6: The REEs results in vein and host rock (μg/g).

REE	Vein							Host rock						
	NY1-4	NY1-5	NY1-10	NY1-13	FY1-19	FY1-28	FY1-30	NY1-4	NY1-5	NY1-10	NY1-13	FY1-19	FY1-28	FY1-30
La	28.60	22.10	6.30	15.50	15.30	16.00	17.40	33.00	31.40	32.70	27.30	32.80	33.10	25.40
Ce	56.30	43.90	11.90	29.40	28.40	27.60	31.70	59.60	56.60	59.10	49.10	62.40	63.80	46.90
Pr	6.42	5.27	1.43	3.49	3.30	3.37	3.64	6.96	6.59	6.14	5.65	7.12	7.37	5.47
Nd	24.40	21.20	5.50	14.10	12.30	13.10	14.70	26.90	24.70	23.50	21.70	28.00	28.90	21.80
Sm	4.17	4.02	0.88	2.56	2.22	2.49	2.92	4.58	4.19	4.23	3.72	4.95	5.35	4.16
Eu	0.91	0.91	0.45	0.55	0.61	0.52	0.68	0.97	0.83	0.87	0.67	0.96	0.99	0.85
Gd	3.75	3.61	0.85	2.10	1.87	2.16	2.51	4.06	3.57	3.57	3.17	4.24	4.54	3.48
Tb	0.66	0.60	0.13	0.36	0.32	0.36	0.45	0.69	0.57	0.60	0.52	0.73	0.78	0.63
Dy	3.28	3.17	0.70	1.85	1.52	1.98	2.37	3.60	2.74	2.97	2.85	3.56	3.98	3.20
Ho	0.59	0.54	0.13	0.33	0.30	0.40	0.46	0.66	0.52	0.57	0.57	0.63	0.73	0.63
Er	1.58	1.40	0.33	0.89	0.85	1.16	1.18	1.82	1.49	1.45	1.60	1.60	2.04	1.70
Tm	0.25	0.23	0.05	0.14	0.13	0.19	0.20	0.30	0.26	0.25	0.30	0.24	0.34	0.27
Yb	1.38	1.21	0.28	0.84	0.75	1.18	1.14	1.83	1.55	1.46	1.79	1.24	1.78	1.60
Lu	0.20	0.18	0.04	0.12	0.10	0.19	0.16	0.25	0.22	0.22	0.24	0.16	0.27	0.22
ΣREE	132.49	108.34	28.97	72.23	67.97	70.70	79.49	145.23	135.23	137.63	119.18	148.65	153.97	116.31
δEu	0.69	0.71	1.57	0.70	0.89	0.67	0.75	0.68	0.64	0.67	0.58	0.63	0.60	0.67

$\delta Eu = 2Eu/(Sm + Gd)^*$ value. Chondrite-normalizing values [66].

Table 7: The REEs results in micritic lamina (μg/g).

	NY1-1	NY1-2	NY1-3	NY1-7	NY1-11	FY1-15	FY1-16	FY1-17
La	21.1	18.5	33.5	20.2	30.4	28.1	16.1	22.8
Ce	38.3	33.5	60.2	36.9	54	55.9	31	46
Pr	4.42	3.89	6.91	4.38	5.94	6.59	3.68	5.44
Nd	16.8	14.4	25.3	16.1	22.5	25.9	14	21.6
Sm	2.97	2.52	4.39	2.94	3.76	4.7	2.65	3.95
Eu	0.699	0.616	0.906	0.648	0.758	0.915	0.651	0.907
Gd	2.69	2.17	3.65	2.65	3.34	3.89	2.22	3.41
Tb	0.452	0.377	0.622	0.427	0.537	0.668	0.385	0.61
Dy	2.3	1.98	3.1	2.19	2.69	3.26	1.99	3.15
Ho	0.448	0.377	0.595	0.393	0.503	0.641	0.39	0.61
Er	1.21	1.01	1.57	1.07	1.32	1.7	1.01	1.56
Tm	0.22	0.17	0.27	0.18	0.21	0.27	0.16	0.26
Yb	1.27	0.966	1.57	1.12	1.26	1.7	1.04	1.64
Lu	0.159	0.145	0.23	0.149	0.181	0.249	0.145	0.223
ΣREE	93.04	80.62	142.81	89.35	127.40	134.48	75.42	112.16
δEu	0.74	0.79	0.67	0.70	0.64	0.64	0.80	0.74

$\delta Eu = 2Eu/(Sm + Gd)^*$ value. Chondrite-normalizing value [66].

[7]. The REE patterns in the veins are consistent with those in host rocks and micritic carbonate laminae, indicating that the materials within the calcite veins may have been derived from the host rock carbonate and micritic laminae.

The trace elements in the micritic laminae, host rocks and veins also exhibit very similar patterns. The concentration of strontium is generally high not only in micritic laminae and host rocks but also in the veins (Figure 11); this is attributed to the dissolved micritic laminae and the host rock with a high Sr ion concentration flowing into diagenetic fluids. During such transfers, precipitation results in the formation of Sr-rich calcite in horizontal fractures. This may explain the high Sr content in the calcite veins [25, 42] and the source of Sr^{2+} for strontianite precipitation. The Ba content is 10456 μg/g in sample FY1-28 owing to the occurrence of barite within the vein (Figure 9(e)). The Es4s in the Dongying Depression develops laminated gypsum mudstone, which is abundant calcium and sulfate ions [24]. Pyrite is packed in the calcite vein (Figure 9(b)), indicating that the sulfate was partially removed during the sulfate reduction reaction [43]. Thus, Liang et al. [44] suggested that gypsum dissolution in the diagenetic fluid increased the concentration of sulfate and resulted in barite precipitation in the fractures. Another possibility is that Ba is universally present in the OM and can be replaced by potassium [45]; thus, sufficient barium may have been liberated from the host rock to facilitate the precipitation of barite.

Therefore, the similar patterns of trace elements and REEs in the micritic laminae, host rocks, and veins indicate that ions that leached from adjacent host rocks and micritic laminae are concentrated in nascent veins because of the focused fluid expulsion along these pathways, after the maturation of OM and the associated generation of organic and carbonic acids. The formation of strontianite and barite is attributed to the contribution of ions from the host rocks and micritic laminae, rather than to the flow of external fluids into the host rock.

5.2.2. C and O Isotopes. The carbon and oxygen isotope compositions of the calcite veins represent the original isotope compositions and specific temperature of the parent fluid precipitation, respectively [5, 46]. However, because of the resetting of $\delta^{18}O$ values during diagenesis in sediments, the initial $\delta^{18}O$ composition of shale with veins cannot be determined [47]. Therefore, the $\delta^{18}O$ values in veins can provide clues regarding the source of the diagenetic fluids and the associated physicochemical conditions [48]. The $\delta^{18}O$ values of most calcite veins are lower than those of the micritic carbonate laminae and carbonates in host rocks (Figure 12); this observation is similar to that made for the coarse-grain calcite veins by Liu et al. [49].

Water–rock interaction during the temperature rise in the rock is likely the major reason for oxygen isotope depletion in the fluids, and thus, it probably influenced the $\delta^{18}O$ of authigenic calcite veins [50, 51]. The oxygen isotopic composition of formation water could have been modified gradually because of oxygen exchange within the silicates of the host rock [52]. Meteoric water infiltration is another mechanism for the negative shift in $\delta^{18}O$ values in the calcite veins. Given the low permeability of the shale and the lack of tectonic uplift [49], the influence of meteoric water infiltration is likely small. Thus, the negative shift in $\delta^{18}O$ more likely results from the modification of the parent fluid via the dehydration of swelling clay minerals and the increase in temperature. The presence of pyrite in a calcite vein may imply that sulfate reductions in the decomposition of OM produced a minor negative shift in $\delta^{18}O$. However, if sulfate reduction occurred in the study area, it would have led to a large

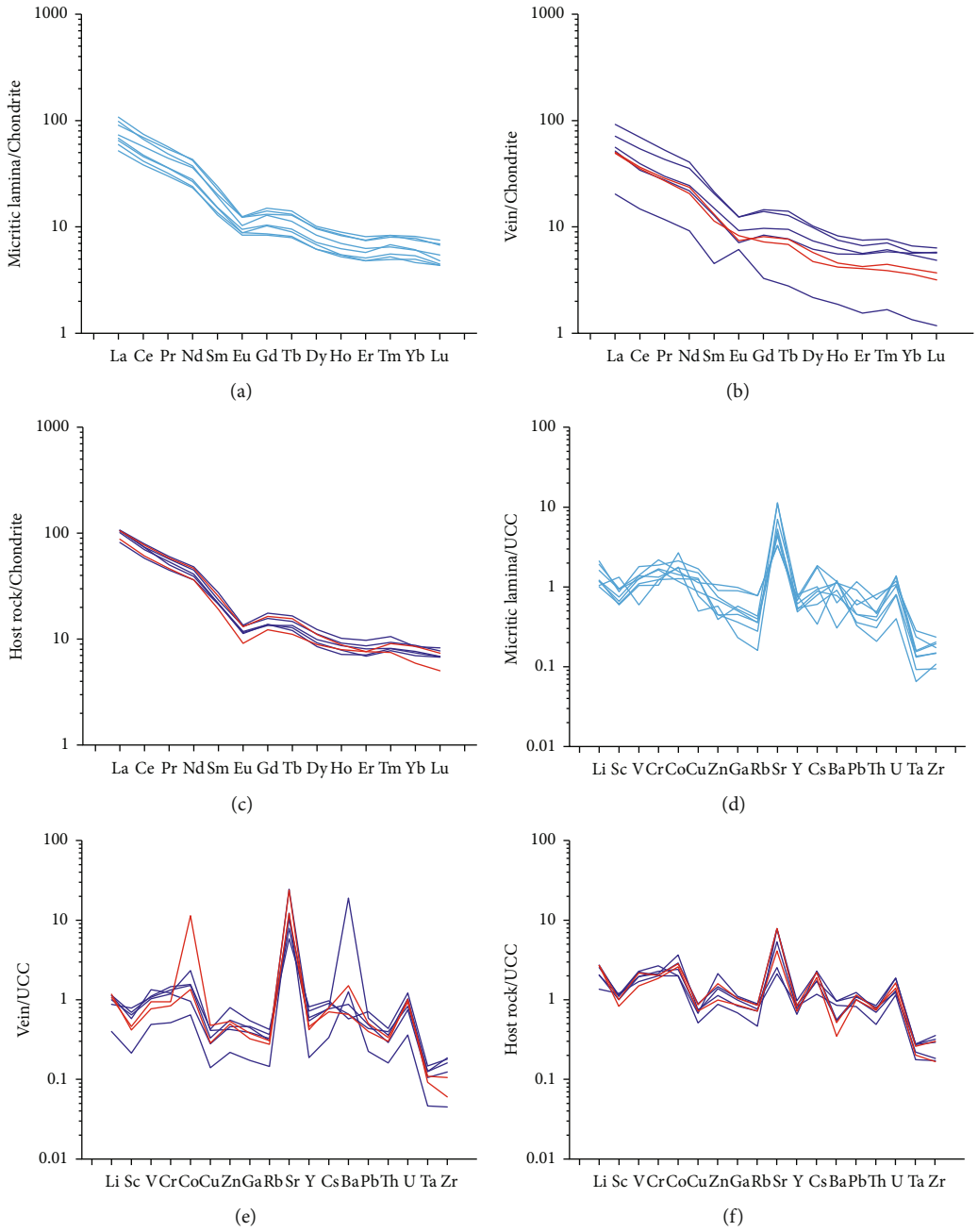

Figure 11: Spider diagram of the ratio of trace elements and the pattern of rare earth elements (REEs). Chondrite-normalized REE patterns in (a) micritic laminae, in (b) veins, and in (c) host rocks. Trace elements normalized by UCC in (a) micritic laminae, in (b) veins, and in (e) host rocks. Blue lines: fibrous calcite and its host rock; red lines: blocky veins and its host rock.

negative shift of carbon isotopes, which does not agree with the results. The $\delta^{18}O$ value of sample NY1-13 collected from a blocky calcite vein is similar to that of its host rock and micritic carbonate laminae. Sample FY1-19 with blocky crystals also has a higher $\delta^{18}O$ value than that of the fibrous veins. This possibly suggests that the blocky veins formed earlier than the fibrous veins.

The majority of the $\delta^{13}C$ values of the fibrous and blocky veins are similar to those of the micritic carbonate laminae, with an average of +3.5‰ VPDB, except for sample NY1-13 that has the lowest $\delta^{13}C$ value (Table 4). The enrichment of ^{13}C in the host rock is induced by exchanges with the dissolved organic carbon [53]. Hence, the host rock carbonate has a lower $\delta^{13}C$ value than the calcite vein; if the carbon isotope composition of the veins is the same as that of host rock carbonate, the incorporation of depleted organic carbon into the carbonate in the host rock can lead to this difference. The depleted organic carbon can be exchanged with any existing veins, but a larger crystal size in veins could have helped maintain their carbon composition, whereas the fine-

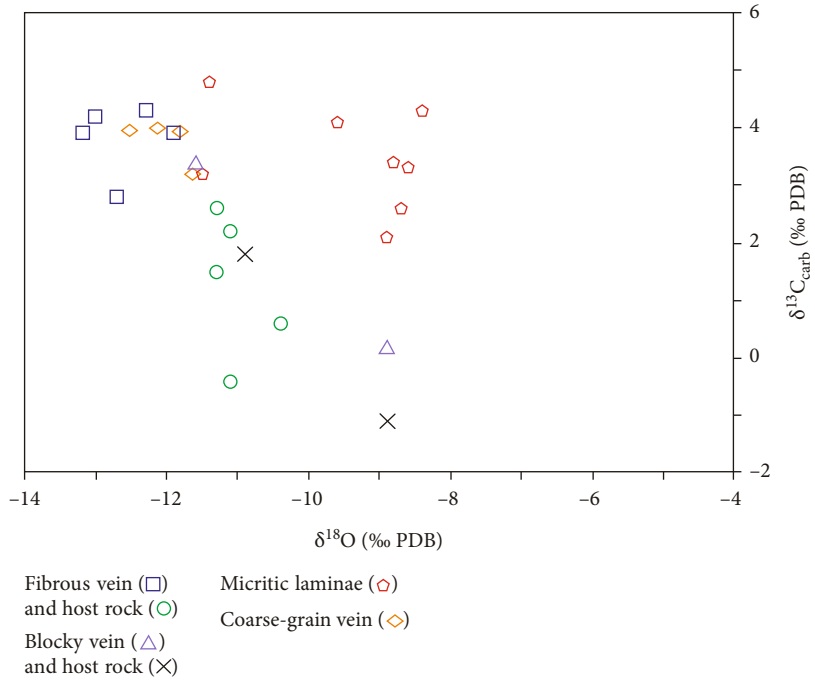

Figure 12: C-O isotopes of micritic laminae, calcite veins, and adjacent host rocks. The data of the coarse-grained vein are from Liu et al. [49].

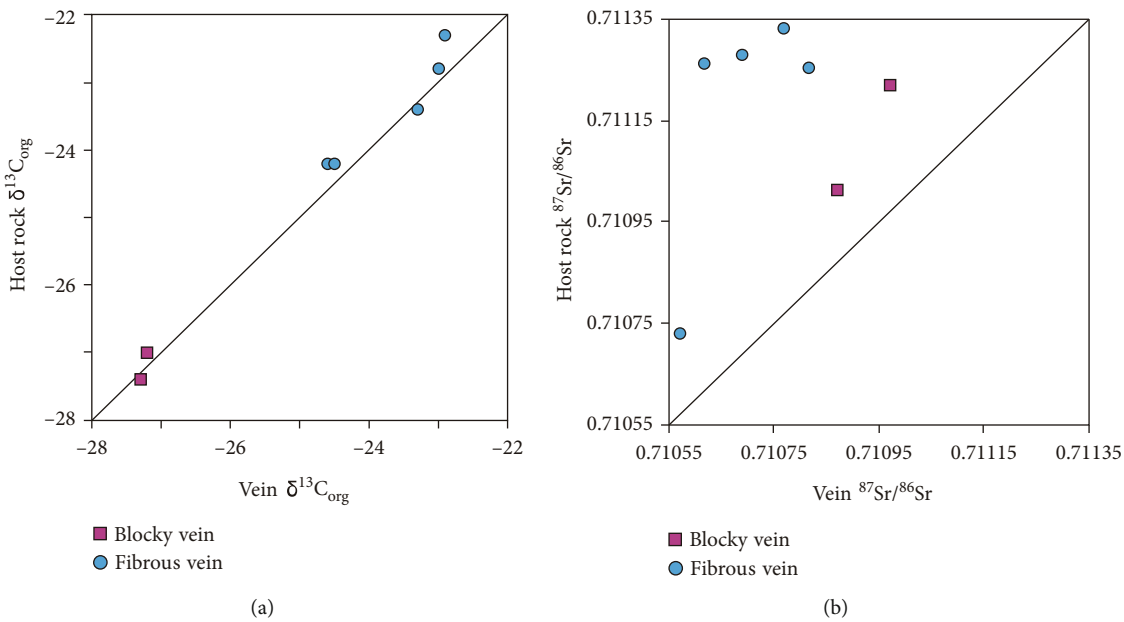

Figure 13: Organic carbon (a) and strontium (b) isotopes of calcite veins and host rocks.

grained carbonate in the host rocks could have been more thoroughly exchanged with the depleted carbon from the OM [53]. The $\delta^{13}C_{org}$ results show that the calcite veins are lighter than the host rocks (Figure 13(a)), which too indicates the exchange of organic carbon with carbonate in host rocks in the burial environment. Blocky veins are related to hydrocarbons, and it would have been easier for OM to fill up blocky crystals (Figures 6(e) and 6(g)); therefore, the organic carbon isotope of blocky veins is lower than that of fibrous veins.

Thus, the carbonate content of the calcite veins is derived from the micritic carbonate dissolution-reprecipitation mechanism. The negative shift of the $\delta^{18}O$ value in calcite veins is mainly caused by the dehydration of swelling clay

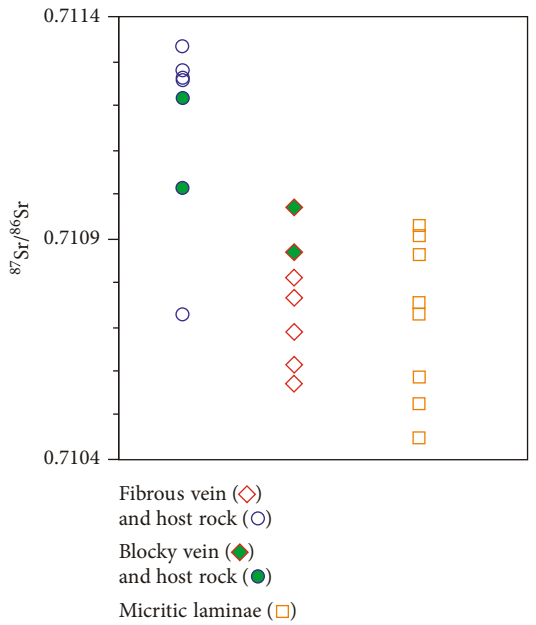

Figure 14: Strontium isotopic composition of micritic carbonate laminae, calcite veins, and host rocks.

minerals during the increase in the burial temperature of the shale. The host rock carbonate with lower $\delta^{13}C$ values results from exchanges with the carbon taken from the OM.

5.2.3. Sr Isotopes. The Sr isotope of calcite veins is another factor that indicates whether the veins grew from local or regional fluids [19]. ^{87}Sr is obtained from the radioactive decay of ^{87}Rb, which is not incorporated into the calcite lattice. Therefore, radioactive decay over time does not affect the Sr isotope of a calcite vein. If the calcite veins were derived from the carbonates in the host rocks, the $^{87}Sr/^{86}Sr$ ratio of the veins and host rock carbonate would be similar. Therefore, by comparing the Sr isotope values in calcite veins and host rocks, it is possible to determine whether the calcite veins formed from local materials or from the advective transport of fluids over a longer distance [20]. The Sr isotopic ratio in the host rock is slightly greater than that in its vein (Figure 13(b)), but still much lower than that in its noncarbonate sections. Perhaps, small amounts of Sr within detrital silicate were exchanged with the carbonate in the host rock, thereby increasing the $^{87}Sr/^{86}Sr$ ratio [54]. The average Sr isotopic composition of micritic carbonate is 0.710718, which may reflect the characteristics of the initial sedimentary environment. The Sr isotopic concentration of the fibrous calcite vein is similar to that of micritic carbonate, indicating that the fluids of the fibrous vein were derived from the micritic carbonate. The isotopic concentration of the blocky calcite veins is also close to those of micritic carbonate or slightly higher than those of fibrous veins, indicating the Sr isotope may be affected by the dehydration of clay minerals in the early stage because the blocky calcite forms earlier than the fibrous calcite (Figure 14). Therefore, the materials in the calcite vein originate from micritic carbonate in the host rock and micritic laminae.

5.3. Formation Mode of Calcite Veins. The rocks from well NY1 and FY1 are in the oil window (Ro > 0.5) and have good hydrocarbon potential. The maturation of the OM leads to the expulsion of organic acid and hydrocarbons and the dehydration of clay minerals, resulting in the dissolution of micritic carbonate and fluid overpressure within the host rocks [3, 27]. These diagenetic fluids within the host rocks migrate to the interlayer via diffusion, forming overpressure fractures and providing space for the later precipitation of calcite veins. The syntaxial veins with blocky crystals are induced by the different growth rates of the individual crystals; they may form in a cracking event, thereby creating enough space for the dissolved carbonate within the host rock to precipitate [7, 55]. The fibrous calcite grows in a narrow fracture, and crystal growth competition is suppressed [11]. The vein-wall interface represents an area with low adhesion and new material accumulation, causing the dilation of the vein because of the force of crystallization of calcite fibers [17]. Moreover, the petrological observation and differences in the oxygen and strontium isotopic concentrations in blocky and fibrous calcite probably indicate that the blocky calcite forms earlier than the fibrous calcite.

Therefore, the migration of the nutrients of the calcite within the host rocks to the interlayer fracture promotes the growth of blocky calcite. Generally, the blocky crystals comprise the clay minerals that detached from the vein walls and the hydrocarbons expulsed upon OM maturation. After the wide fracture is filled with the blocky vein, the vertical migration of fluids is hindered causing the dissolved carbonate to gradually precipitate into fibrous calcite in the vein-wall interface (Figure 15(a)). Besides, the hydrocarbon-bearing fluid contributes to the formation of bedding-parallel fractures in the transitional surface of micritic carbonate lamina and organic-rich clay lamina and interlayer within rocks, and this in turn results in the growth and continuous dilation of fibrous crystals (Figure 15(b)) [56].

5.4. Significance of Calcite Veins for Shale Oil. The Es4s–Es3x rocks were deposited in a semideep and deep lacustrine environment. Compared with the marine shale in China, the TOC and carbonate mineral contents are considerably higher in the Es4s–Es3x rocks [57–60]. Moreover, compared with some major shale in the United States, the Es4s–Es3x shale has deep burial depth, low thermal maturity, high carbonate content, and low quartz content. These differences affect the types of pores in the Es4s–Es3x shale [59, 61, 62]. Therefore, unlike marine gas shale with primarily OM pores, the carbonate recrystallization intercrystalline pores and dissolution pores are the main pores in the Es4s–Es3x shale [24]. Moreover, the pores are mainly concentrated in the laminated interface near the veins; further, there exists favorable horizontal connectivity along a given lamina because of the connection of microfractures [49].

Therefore, the shale with a bedding-parallel calcite vein is considered a high-quality reservoir, characterized by high TOC and hydrocarbon potential, abundant recrystallization intercrystalline pores and interlaminar fractures, and high

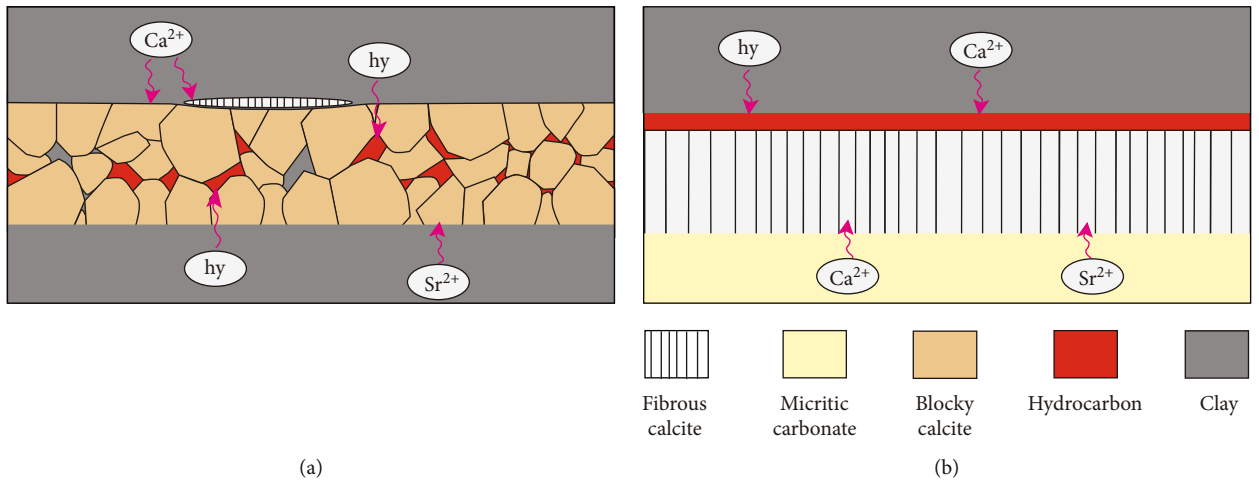

Figure 15: Pattern of hydrocarbon accumulation of blocky and fibrous veins (hy: hydrocarbon).

content of brittle minerals (average greater than 70%) [61, 63]. The shale with veins is the favorable lithofacies for shale oil reservoirs and a sweet spot for exploration [64].

6. Conclusions

(1) Bedding-parallel calcite veins are widespread in source rocks in the Dongying Depression. Antitaxial and syntaxial calcite veins can be distinguished through petrographic observations. Antitaxial veins typically contain fibrous crystals that grow almost perpendicular to the host rocks with smooth fiber boundaries. The median zone of antitaxial veins is often initial micritic carbonate. Calcite in syntaxial veins develops blocky morphologies with various sizes and clear crystal growth competition

(2) The shale mineralogy of NY1 and FY1 has high carbonate and low feldspar content. The shale has been buried almost in the oil window and has good hydrocarbon potential. With increasing depth, the OM generates acidic fluids to dissolve carbonate. The mixed illite/smectite also transforms into illite. Consequently, the formation of spaces in the transitional lithology and interlayer within rocks and fluid overpressure is promoted

(3) The similar trace element and REE patterns in the micritic laminae, host rocks, and veins indicate that the ions leached from the adjacent host rocks and micritic laminae are concentrated in the nascent veins. This concentration is attributed to focused fluid expulsion along these pathways after the OM matures and produces organic and carbonic acids. Further, the Sr and Ba for the precipitation of strontianite and barite, respectively, originated from the host rocks rather than from the external fluids

(4) The host rock carbonate is enriched in ^{87}Sr and depleted in ^{13}C. This is caused by isotopic exchanges with the noncarbonate host rock components. The micritic carbonate lamina grows as the median zone along with the fibrous calcite, probably reflecting the nature of the vein-forming fluids. The carbon and strontium isotopic compositions of micritic laminae and veins are also very similar. The negative shift of the oxygen isotopes of the veins is induced by the dehydration of clay minerals and the increase in temperature. This indicates that the materials of the veins are derived from the dissolution of carbonate within the shale in a closed system

(5) The migration of the diagenetic fluid is vertical and limited in the interlayer. Such migration promotes the growth of calcite fibers by crystallization. Blocky crystals rapidly grow from both sides of the fracture toward the center, allowing the hydrocarbons from the host rocks to occupy the intercrystalline pores. In addition, the shale with bedding-parallel calcite vein is the favorable lithofacies for shale oil reservoirs

Data Availability

The clay minerals data used to support the findings of this study have been deposited in Figure 4 repository (doi:10.1016/j.marpetgeo.2016.02.022; doi:10.1016/j.marpetgeo.2016.12.004). The C-O isotopes of coarse-grained vein data used to support the findings of this study have been deposited in Figure 12 repository (doi:10.1007/s12583-016-0946-3). The TOC, δ13Ccarb, δ18O, δ13Corg, 87Sr/86Sr, trace elements and REEs data used to support the findings of this study are included within the article. The XRD analysis, TOC content, and Rock-Eval parameters of rocks data used to support the findings of this study were supplied by the Shengli Oilfield Company, SINOPEC, under license and so cannot be made freely available. Requests for access to these data should be made to Zhenhuan Shen (shenzh9311@163.com).

Conflicts of Interest

The authors declare that they have no conflicts of interest.

Acknowledgments

We appreciate the Laboratory of Geological Microbiology at China University of Geosciences (Beijing) and the Analytical Laboratory at Beijing Research Institute of Uranium Geology for sample analysis. This paper is supported by the National Program on Chinese Fundamental Research Funds for the Central Universities (2652019079) and Key Basic Research Project of China (2014CB239102).

References

[1] P. R. Cobbold, A. Zanella, N. Rodrigues, and H. Løseth, "Bedding-parallel fibrous veins (beef and cone-in-cone): worldwide occurrence and possible significance in terms of fluid overpressure, hydrocarbon generation and mineralization," *Marine and Petroleum Geology*, vol. 43, pp. 1–20, 2013.

[2] J. F. W. Gale, S. E. Laubach, J. E. Olson, P. Eichhubl, and A. Fall, "Natural fractures in shale: a review and new observations," *AAPG Bulletin*, vol. 98, no. 11, pp. 2165–2216, 2014.

[3] J. Zhang, Z. Jiang, X. Jiang, S. Wang, C. Liang, and M. Wu, "Oil generation induces sparry calcite formation in lacustrine mudrock, Eocene of East China," *Marine and Petroleum Geology*, vol. 71, pp. 344–359, 2016.

[4] P. D. Bons and M. Montenari, "The formation of antitaxial calcite veins with well-developed fibres, Oppaminda Creek, South Australia," *Journal of Structural Geology*, vol. 27, no. 2, pp. 231–248, 2005.

[5] Q. Meng, J. Hooker, and J. Cartwright, "Early overpressuring in organic-rich shales during burial: evidence from fibrous calcite veins in the lower jurassic shales-with-beef member in the Wessex Basin, UK," *Journal of the Geological Society*, vol. 174, no. 5, pp. 869–882, 2017.

[6] D. W. Durney and J. G. Ramsay, "Incremental strains measured by syntectonic crystal growths," in *Gravity and Tectonics*, K. A. Jong and R. Scholten, Eds., pp. 67–97, Wiley, New York, 1973.

[7] P. D. Bons, M. A. Elburg, and G. R. Enrique, "A review of the formation of tectonic veins and their microstructures," *Journal of Structural Geology*, vol. 43, pp. 33–62, 2012.

[8] S. Spencer, "The use of syntectonic fibres to determine strain estimates and deformation paths: an appraisal," *Tectonophysics*, vol. 194, no. 1-2, pp. 13–34, 1991.

[9] J. G. Ramsay, "The crack-seal mechanism of rock deformation," *Nature*, vol. 284, no. 5752, pp. 135–139, 1980.

[10] S. F. Cox and M. A. Etheridge, "Crack-seal fibre growth mechanism and their significance in the development of oriented layer silicate microstructures," *Journal of Structural Geology*, vol. 92, pp. 147–170, 1983.

[11] C. Hilgers, D. Köhn, P. D. Bons, and J. L. Urai, "Development of crystal morphology during unitaxial growth in a progressively widening vein: II. Numerical simulations of the evolution of antitaxial fibrous veins," *Journal of Structural Geology*, vol. 23, no. 6-7, pp. 873–885, 2001.

[12] P. R. Cobbold and N. Rodrigues, "Seepage forces, important factors in the formation of horizontal hydraulic fractures and bedding-parallel fibrous veins (?beef? and ?cone-in-cone?)," *Geofluids*, vol. 7, no. 3, pp. 313–322, 2007.

[13] A. Zanella, P. R. Cobbold, and T. Boassen, "Natural hydraulic fractures in the Wessex Basin, SW England: widespread distribution, composition and history," *Marine and Petroleum Geology*, vol. 68, pp. 438–448, 2015.

[14] W. D. Means and T. Li, "A laboratory simulation of fibrous veins: some first observations," *Journal of Structural Geology*, vol. 23, no. 6-7, pp. 857–863, 2001.

[15] D. V. Wiltschko and J. W. Morse, "Crystallization pressure versus "crack seal" as the mechanism for banded veins," *Geology*, vol. 29, no. 1, pp. 79–82, 2001.

[16] C. Hilgers and J. L. Urai, "Microstructural observations on natural syntectonic fibrous veins: implications for the growth process," *Tectonophysics*, vol. 352, no. 3-4, pp. 257–274, 2002.

[17] C. Hilgers and J. L. Urai, "On the arrangement of solid inclusions in fibrous veins and the role of the crack-seal mechanism," *Journal of Structural Geology*, vol. 27, no. 3, pp. 481–494, 2005.

[18] N. Rodrigues, P. R. Cobbold, H. Loseth, and G. Ruffet, "Widespread bedding-parallel veins of fibrous calcite ('beef') in a mature source rock (Vaca Muerta Fm, Neuquén Basin, Argentina): evidence for overpressure and horizontal compression," *Journal of the Geological Society*, vol. 166, pp. 695–709, 2011.

[19] M. A. Elburg, P. D. Bons, J. Foden, and C. W. Passchier, "The origin of fibrous veins: constraints from geochemistry," *Geological Society, London, Special Publications*, vol. 200, no. 1, pp. 103–118, 2002.

[20] A. M. McCaig, D. M. Wayne, J. D. Marshall, D. Banks, and I. Henderson, "Isotopic and fluid inclusion studies of fluid movement along the Gavarnie thrust, Central Pyrenees; reaction fronts in carbonate mylonites," *American Journal of Science*, vol. 295, no. 3, pp. 309–343, 1995.

[21] N. H. S. Oliver and P. D. Bons, "Mechanisms of fluid flow and fluid-rock interaction in fossil metamorphic hydrothermal systems inferred from vein-wallrock patterns, geometry and microstructure," *Geofluids*, vol. 1, no. 2, pp. 137–162, 2001.

[22] D. M. Fisher, S. L. Brantley, M. Everett, and J. Dzvonik, "Cyclic fluid flow through a regionally extensive fracture network within the Kodiak accretionary prism," *Journal of Geophysical Research-Solid Earth*, vol. 100, no. B7, pp. 12881–12894, 1995.

[23] C. Ma, C. Dong, G. Luan, C. Lin, X. Liu, and D. Elsworth, "Types, characteristics and effects of natural fluid pressure fractures in shale: a case study of the Paleogene strata in eastern China," *Petroleum Exploration and Development*, vol. 43, no. 4, pp. 634–643, 2016.

[24] C. Liang, Y. Cao, Z. Jiang, J. Wu, S. Guoqi, and Y. Wang, "Shale oil potential of lacustrine black shale in the Eocene Dongying Depression: implications for geochemistry and reservoir characteristics," *AAPG Bulletin*, vol. 101, no. 11, pp. 1835–1858, 2017.

[25] C. Bai, B. Yu, H. Liu et al., "The genesis and evolution of carbonate minerals in shale oil formations from Dongying Depression, Bohai Bay basin, China," *International Journal of Coal Geology*, vol. 189, pp. 8–26, 2018.

[26] M. Wang, Y. Chen, G. Song et al., "Formation of bedding-parallel, fibrous calcite veins in laminated source rocks of the Eocene Dongying Depression: a growth model based on petrographic observations," *International Journal of Coal Geology*, vol. 200, pp. 18–35, 2018.

[27] X. Guo, S. He, K. Liu, G. Song, X. Wang, and Z. Shi, "Oil generation as the dominant overpressure mechanism in the Cenozoic Dongying Depression, Bohai Bay basin, China," *AAPG Bulletin*, vol. 94, no. 12, pp. 1859–1881, 2010.

[28] Y. L. Feng, S. T. Li, and Y. C. Lu, "Sequence stratigraphy and architectural variability in late Eocene lacustrine strata of the

Dongying Depression, Bohai Bay basin, eastern China," *Sedimentary Geology*, vol. 295, pp. 1–26, 2013.

[29] X. Gu, K. Liu, S. He et al., "Petroleum generation and charge history of the northern Dongying Depression, Bohai Bay basin, China: insight from integrated fluid inclusion analysis and basin modelling," *Marine and Petroleum Geology*, vol. 32, no. 1, pp. 21–35, 2012.

[30] Z. Chen, W. Huang, Q. Liu, L. Zhang, and S. Zhang, "Geochemical characteristics of the paleogene shales in the Dongying Depression, eastern China," *Marine and Petroleum Geology*, vol. 73, pp. 249–270, 2016.

[31] Y. Li, J. Cai, X. Wang, Y. Hao, and Q. Liu, "Smectite-illitization difference of source rocks developed in saline and fresh water environments and its influence on hydrocarbon generation: a study from the Shahejie formation, Dongying Depression, China," *Marine and Petroleum Geology*, vol. 80, pp. 349–357, 2017.

[32] W. Ding, C. Li, C. Y. Li, K. Jiu, W. Zeng, and L. Wang, "Fracture development in shale and its relationship to gas accumulation," *Geoscience Frontiers*, vol. 3, no. 1, pp. 97–105, 2012.

[33] W. Zeng, J. Zhang, W. Ding et al., "Fracture development in Paleozoic shale of Chongqing area (South China). Part one: fracture characteristics and comparative analysis of main controlling factors," *Journal of Asian Earth Science*, vol. 75, pp. 251–266, 2013.

[34] A. Ougier-Simonin, F. Renard, C. Boehm, and S. Vidal-Gilbert, "Microfracturing and microporosity in shales," *Earth-Science Reviews*, vol. 162, pp. 198–226, 2016.

[35] K. Jiu, W. Ding, W. Huang, Y. Zhang, S. Zhao, and L. Hu, "Fractures of lacustrine shale reservoirs, the Zhanhua Depression in the Bohai Bay basin, eastern China," *Marine and Petroleum Geology*, vol. 48, pp. 113–123, 2013.

[36] T. Barth and K. Bjørlykke, "Organic acids from source rock maturation: generation potentials, transport mechanisms and relevance for mineral diagenesis," *Applied Geochemistry*, vol. 8, no. 4, pp. 325–337, 1993.

[37] A. Shemesh, H. Ron, Y. Erel, Y. Kolodny, and A. Nur, "Isotopic composition of vein calcite and its fluid inclusions: implication to paleohydrological systems, tectonic events and vein formation processes," *Chemical Geology*, vol. 94, no. 4, pp. 307–314, 1992.

[38] G. R. Helz and H. D. Holland, "The solubility and geologic occurrence of strontianite," *Geochimica et Cosmochimica Acta*, vol. 29, no. 12, pp. 1303–1315, 1965.

[39] L. B. Aspler, J. R. Chiarenzelli, and B. L. Cousens, "Fluvial, lacustrine and volcanic sedimentation in the Angikuni subbasin, and initiation of ~1.84-1.79 Ga Baker Lake Basin, western Churchill Province, Nunavut, Canada," *Precambrian Research*, vol. 129, no. 3-4, pp. 225–250, 2004.

[40] J. S. Hanor, "Barite–celestine geochemistry and environments of formation," *Reviews in Mineralogy and Geochemistry*, vol. 40, no. 1, pp. 193–275, 2000.

[41] M. Bau and P. Möller, "Rare earth element fractionation in metamorphogenic hydrothermal calcite, magnesite and siderite," *Mineralogy and Petrology*, vol. 45, no. 3-4, pp. 231–246, 1992.

[42] L. A. Derry, "A burial diagenesis origin for the Ediacaran Shuram-Wonoka carbon isotope anomaly," *Earth and Planetary Science Letters*, vol. 294, no. 1-2, pp. 152–162, 2010.

[43] M. E. Torres, H. J. Brumsack, G. Bohrmann, and K. C. Emeis, "Barite fronts in continental margin sediments: a new look at barium remobilization in the zone of sulfate reduction and formation of heavy barites in diagenetic fronts," *Chemical Geology*, vol. 127, no. 1-3, pp. 125–139, 1996.

[44] C. Liang, J. Wu, Z. Jiang, Y. Cao, and G. Song, "Sedimentary environmental controls on petrology and organic matter accumulation in the upper fourth member of the Shahejie formation (Paleogene, Dongying Depression, Bohai Bay basin, China)," *International Journal of Coal Geology*, vol. 186, pp. 1–13, 2018.

[45] E. M. Griffith and A. Paytan, "Barite in the ocean - occurrence, geochemistry and palaeoceanographic applications," *Sedimentology*, vol. 59, no. 6, pp. 1817–1835, 2012.

[46] S. Boggs, *Petrology of Sedimentary Rocks*, Cambridge University Press, Cambridge, 2009.

[47] R. Worden, M. Benshatwan, G. Potts, and S. Elgarmadi, "Basin-scale fluid movement patterns revealed by veins: Wessex Basin, UK," *Geofluids*, vol. 16, pp. 149–174, 2015.

[48] D. Conybeare and H. Shaw, "Fracturing, overpressure release and carbonate cementation in the Everest Complex, North Sea," *Clay Minerals*, vol. 35, no. 1, pp. 135–149, 2000.

[49] H. Liu, S. Zhang, G. Song et al., "A discussion on the origin of shale reservoir inter-laminar fractures in the Shahejie Formation of Paleogene, Dongying Depression," *Journal of Earth Science*, vol. 28, no. 6, pp. 1064–1077, 2017.

[50] F. J. Longstaffe, "Oxygen isotope studies of diagenesis in the basal Belly River sandstone, Pembina I-Pool, Alberta," *Journal of Sedimentary Research*, vol. 56, pp. 78–88, 1986.

[51] Y. Zheng and J. Hoefs, "Carbon and oxygen isotopic covariations in hydrothermal calcites," *Mineralium Deposita*, vol. 28, pp. 79–89, 1993.

[52] H. W. Yeh and S. M. Savin, "Mechanism of burial metamorphism of argillaceous sediments: 3. O-isotope evidence," *Geological Society of America Bulletin*, vol. 88, no. 9, pp. 1321–1330, 1977.

[53] J. N. Hooker, J. Cartwright, B. Stephenson, C. R. P. Silver, A. J. Dickson, and Y. T. Hsieh, "Fluid evolution in fracturing black shales, Appalachian Basin," *AAPG Bulletin*, vol. 101, no. 8, pp. 1203–1238, 2017.

[54] C. Hilgers and S. Sindern, "Textural and isotopic evidence on the fluid source and transport mechanism of antitaxial fibrous microstructures from the Alps and the Appalachians," *Geofluids*, vol. 5, no. 4, pp. 239–250, 2005.

[55] C. Liang, Y. Cao, K. Liu, Z. Jiang, J. Wu, and F. Hao, "Diagenetic variation at the lamina scale in lacustrine organic-rich shales: implications for hydrocarbon migration and accumulation," *Geochimica et Cosmochimica Acta*, vol. 229, pp. 112–128, 2018.

[56] C. J. L. Wilson, "Crystal growth during a single-stage opening event and its implications for syntectonic veins," *Journal of Structural Geology*, vol. 16, no. 9, pp. 1283–1296, 1994.

[57] Y. Bai, L. Ma, W. J. Wu, and Y. Ma, "Geological characteristics and resource potential of oil shale in Ordos Basin (in Chinese with English abstract)," *Geology in China*, vol. 36, pp. 1123–1137, 2009.

[58] F. Hao, H. Zou, and Y. Lu, "Mechanisms of shale gas storage: implications for shale gas exploration in China," *AAPG Bulletin*, vol. 97, no. 8, pp. 1325–1346, 2013.

[59] M. Wang, L. Shi, W. Wang, A. Huang, G. Chen, and S. Tian, "Comparative study on geochemical characteristics of shale oil between China and U.S.a. (in Chinese with English abstract)," *Lithologic Reservoirs*, vol. 26, pp. 67–74, 2014.

[60] H. Nie, P. Zhang, R. Bian, X. Wu, and C. Zhai, "Oil accumulation characteristics of China continental shale (in Chinese with English abstract)," *Earth Science Frontiers*, vol. 23, pp. 55–62, 2016.

[61] D. M. Jarvie, R. J. Hill, T. E. Ruble, and R. M. Pollastro, "Unconventional shale-gas systems: the Mississippian Barnett Shale of north-central Texas as one model for thermogenic shale-gas assessment," *AAPG Bulletin*, vol. 91, no. 4, pp. 475–499, 2007.

[62] Y. Yang, C. Liang, J. Zhang, Z. Jiang, and X. Tang, "A developmental model of lacustrine shale gas genesis: a case from T3y7 shale in the Ordos Basin, China," *Journal of Natural Gas Science and Engineering*, vol. 22, pp. 395–405, 2015.

[63] S. L. Montgomery, D. M. Jarvie, K. A. Bowker, and R. M. Pollastro, "Mississippian Barnett shale, Fort Worth basin, north-Central Texas: gas-shale play with multi-trillion cubic foot potential," *AAPG Bulletin*, vol. 89, no. 2, pp. 155–175, 2005.

[64] S. Zhang, H. Liu, Y. Liu et al., "Main controls and geological sweet spot types in Paleogene shale oil rich areas of the Jiyang Depression, Bohai Bay basin, China," *Marine and Petroleum Geology*, vol. 111, pp. 576–587, 2020.

[65] S. R. Taylor and S. M. McLennan, "The geochemical evolution of the continental crust," *Reviews of Geophysics*, vol. 33, no. 2, pp. 241–265, 1995.

[66] W. V. Boynton, "Geochemistry of the rare earth elements: meteorite studies," in *Rare earth element geochemistry*, P. Henderson, Ed., pp. 63–114, Elsevier, 1984.